SCHOOL *of*
GRADUATE STUDIES
EAST TENNESSEE STATE UNIVERSITY

East Tennessee State University
Digital Commons @ East Tennessee State University

Electronic Theses and Dissertations

Student Works

8-2007

A Computational Chemistry Study of Spin Traps.

Jacob Fosso-Tande
East Tennessee State University

Follow this and additional works at: https://dc.etsu.edu/etd

Part of the Analytical Chemistry Commons, and the Numerical Analysis and Scientific Computing Commons

A Computational Chemistry Study of Spin Traps

_____

A thesis

presented to

the faculty of the Department of Chemistry

East Tennessee State University

in partial fulfillment

of the requirements for the degree

Master of Science in Chemistry

_____

by

Jacob Fosso Tande

August 2007

_____

Dr. Scott Kirkby, Chair

Dr. Jeffery Wadeska

Dr. David Close

ABSTRACT

A Computational Chemistry Study of Spin Traps

by

Jacob Fosso Tande

Many defects in physiological processes are due to free radical damage: reactive oxygen species, nitric oxide, and hydroxyl radicals have been implicated in the parthenogenesis of cancer, diabetes mellitus, and rheumatoid arthritis. We herein characterize the *phenyl-N-ter-butyl nitrone (*PBN) type spin traps in conjunction with the most studied *dimethyl-1-pyrroline-N-oxide* (DMPO) type spin traps using the hydroxyl radical. In this study, theoretical calculations are carried out on the two main types of spin traps (DMPO and PBN) at the density functional theory level (DFT). The energies of the optimized structures, hyperfine calculations in gaseous and aqueous phases of the spin traps and the hydroxyl radical adduct are calculated at the B3LYP correlation and at the 6-31G (d) and 6-311G (2df, p) basis sets respectively. The dielectric effect on the performance of the spin trap is determined using the polarized continuum model. Calculations show a localization of spin densities in both cases. However, DMPO spin traps are shown to be more stable and more interactive in aqueous environment.

ACKNOWLEGMENTS

CONTENTS   Page

Chapter

LIST OF FIGURES

CHAPTER 1

INTRODUCTION

Free radicals are involved in many areas of chemistry, from oxidation processes, combustion reactions, organic synthesis, and biochemistry. The results of these reactions are both the intended products as well as numerous side reactions. In particular, many defects in physiological processes have been attributed to free radical damage. Free radicals have a very short lifetime and will react essentially immediately when formed. As such, biologists and chemists have devised indirect ways to study free radicals. One method consists of using molecules that are capable of reacting with radicals such that the resulting product can be detected by some means, usually Electron Paramagnetic Resonance (EPR) spectroscopy. The molecule that reacts with the free radical is known as a probe. The resulting product is commonly referred to as an adduct because it is a combination of the free radical and the probe. If the adduct is also a radical, it may be characterized using EPR spectroscopy. As such, the probe is referred to as a "spin trap" because it has trapped and preserved the unpaired spin for a longer lifetime. This work seeks to theoretically characterize the phenyl–N–ter–butyl nitrone (PBN) type spin traps and set a basis for comparison with the dimethyl-1–pyrroline–N–oxide (DMPO) type spin trap counterparts.

The importance of the numerous applications in chemical as well as biological systems of spin traps cannot be over emphasized. Not only are spin traps known to capture radicals, but PBN is also known to inhibit free radical release in brain concussion. In *vivo* or in *vitro* administration of nitrone spin trapping compounds, such as PBN, reduces age related deficits. Also, PBN act as an antioxidant for low density lipoproteins [1].

Spin traps were developed as a result of numerous innovations in the detection and characterization of free radicals. Until 1945 not much was known about radicals until the first electron spin resonance (EPR) experiment by Zavoiskii in Russia. Later on in

1954, Fraenkel, Hirshon, and Walling first reported an EPR spectrum recorded during a polymerization process using a number of cross-linked vinyl polymers [2]. Venkataran and Franekel observed in 1955 that isotropic hyperfine structure arose from methyl proton in substituted semiquinone.

Thereafter, detection and determination of radicals has witnessed a continuous improvement due to the advent of more sophisticated electronic equipment and, above all, the use of spin traps.

Numerous publications show that spin traps may be divided into two classes: PBN-type and DMPO-type [14]. These two classes are both nitrones. Unlike the DMPO-type spin traps, which are highly characterized, both theoretically and experimentally, almost nothing is known about the hyperfine properties of the PBN-type spin traps. Figure 1.1 shows the structures of the two main classes of spin traps.

DMPO-type nitrone   PBN-type nitrone
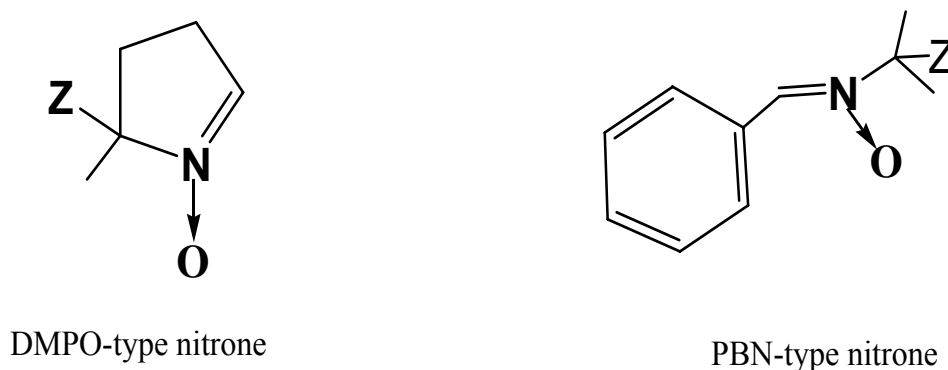
Figure 1.1: Structures of the Two Main Classes of Spin Traps. (Z represents different constituents and the arrow indicates the dative covalent bond.)

Several PBN–type nitrones have been synthesized among which are α-substituted methoxy, amino, cyano, and mercapto nitrones [3, 4] as well as the carboxyl derivatives and the alkoxy phosphoryl [5] derivative. The known DMPO-type spin traps include the alkoxyphosphoryllated nitrones, 5-diethoxyphosphoryl-5-methyl-1-pyrroline-N –oxide (DEPMPO) [7-9], alkoxycarbonyl nitrones 5-ethoxycarbonyl-5-methyl-1-pyrroline N-oxide (EMPO) [11-16] and 5-butoxycarbonyl-5-methyl-1-pyrroline N-oxide (Boc-MPO)

[14]. Based on both theoretical and experimental studies, PBN-type and DMPO-type nitrones have been shown to have spin trapping capabilities. Nevertheless, they have certain limitations: PBN-type nitrones are limited by their capacity to distinguish among radicals where as the DMPO-type nitrones are limited by the stability of the adducts formed and the overall spin trapping efficiency [14].

The spin trapping technique involves the addition of reactive free radicals across the double bond of a diamagnetic spin trap to form a much more stable free radical, the radical adduct, which can then be examined using electron paramagnetic resonance spectroscopy.
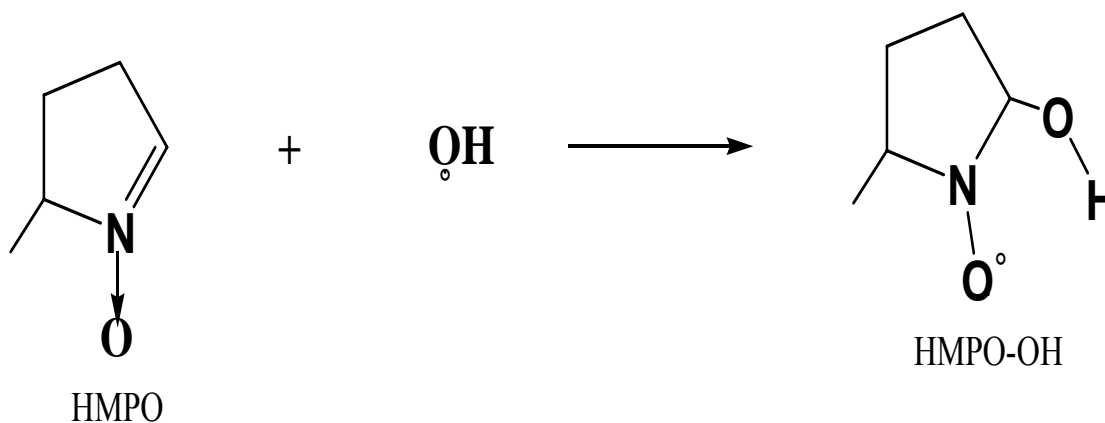
Figure 1.2: Formation of the HMPH-OH Radical Adduct from HMPO and a Hydroxyl Radical.
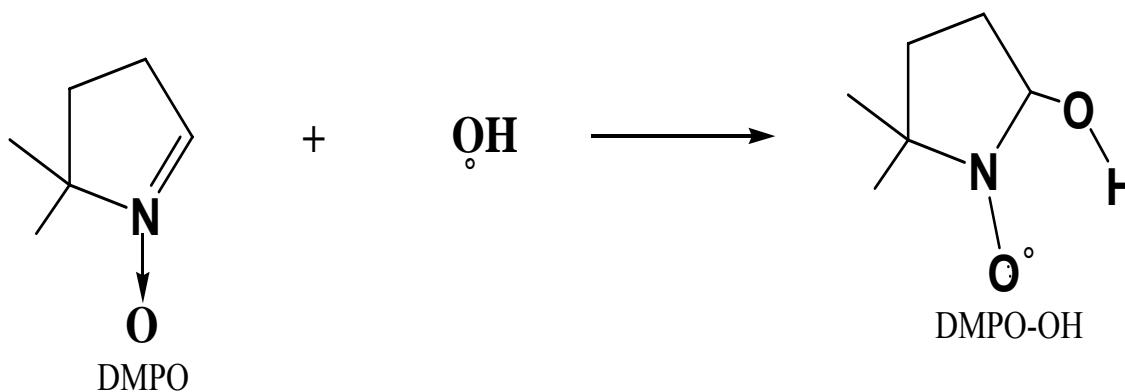
Figure 1.3: Formation of DMPO-OH.
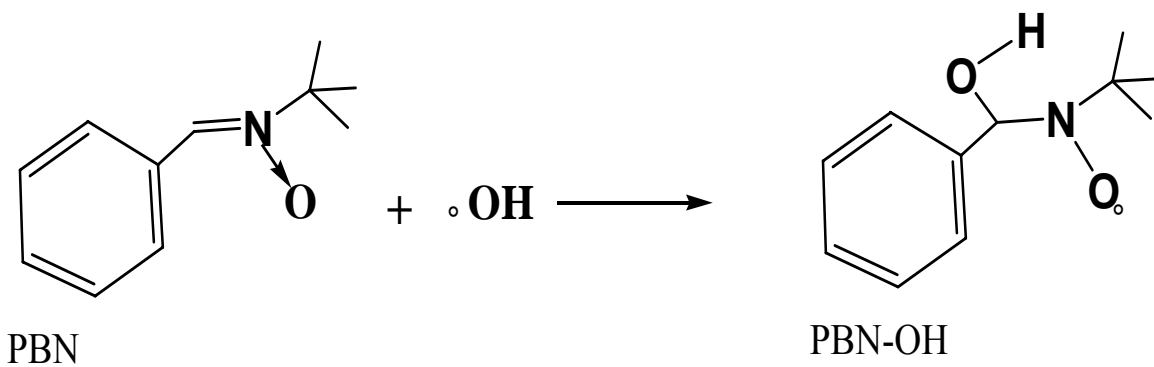
Figure 1.4: Formation of PBN-OH.
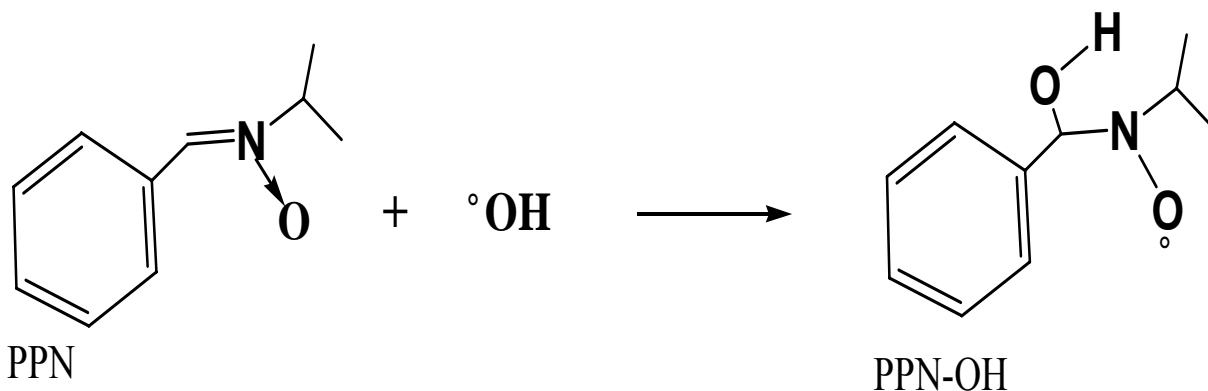
Figure 1.5: Formation of PPN-OH.

Numerous spin traps are now available for the detection and quantification of different free radical species in both chemical and biological systems. Some of the radicals most often found in biological systems are the hydroxyl, oxygen, peroxyl, carbonyl, and sulfurnyl radicals. Some spin traps have been reported as being particularly sensitive to the detection of some radicals [21]. DMPO has been shown to be capable of detecting hydrogen radical [17] in simple chemical radical generating systems under favorable conditions. DEPMPO has equally been shown to be particularly versatile. It

traps hydroxyl, peroxyl and hydrogen radicals and is very successful at detecting hydrogen radicals even in complicated biological free radical generating systems. This was, in fact, the first experiment to show the production of hydrogen radical in plants [21]. It was possible to prove the existence of hydrogen radicals because of the possibility of a comparative study of the EPR spectra of the adducts of the same spin trap in simple electrochemical and complex biological systems. Furthermore, AMPO has been shown, theoretically and experimentally, to posses spin trapping capacity [19] and possible mechanisms for the formation of the $AMPO - O_2H$ radical adduct has been established.

The adduct resulting from the addition of a reactive free radical to the spin trap is by itself a more stable radical. Radicals are of six types:

1. Free radicals: molecules containing one unpaired electron.
2. Biradical: they are molecules containing two unpaired electrons sufficiently remote from each other so that interaction between them is weak.
3. Triplet-state entities: they are species that contain two unpaired electrons with strong interaction. The triplet-state may be the ground state or some optically or thermally excited state.
4. Entities with three or more unpaired electrons
5. Point defects in solids or localized crystal imperfections (one or more electrons may trap at or near these defects and thus give rise to an entity with unpaired electrons)
6. Most transition-metal ions and rare-earth ions.

Among the above systems, the radical adduct falls in the first type. The unpaired electron, giving rise to paramagnetism, is concentrated in a molecular orbital that spreads over more than one atom. The spread out of the single electron depend on the structure of the molecule. The distribution of the unpaired electron can be determined with the use of EPR spectroscopy.

CHAPTER 2

QUANTUM MECHANICS

2.1. EPR Theory

EPR has been used for over fifty years to study variety of paramagnetic species. It
is a technique that permits the investigator to detect and, in favorable cases, characterize
molecules with unpaired electrons without altering or destroying the molecules. As the
name implies, "electron spin" is very important for a better understanding of the EPR
concept. Spin refers to the intrinsic angular momentum from relativistic effects of
electrons. Hund's rule of maximum multiplicity requires that no two electrons in a
molecule can have identical states. Most molecules (organic and inorganic) contain an
even number of electrons and will tend to behave as diamagnetic substances. A naïve but
useful mental picture of the electron can be thought of as spinning negative charge.
Because moving charges generate magnetic field, the electron are thus tiny magnets
moving about randomly. In the presence of an external magnetic field, the tiny magnets
will line up. Figure 2.1 shows the effect of a magnetic field on electrons.
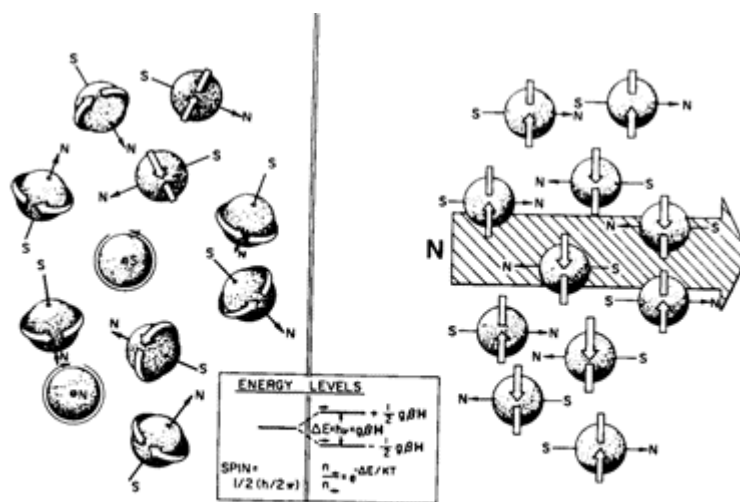
Figure 2. 1: Effect of Magnetic Field on Spinning Electrons [18]

EPR spectroscopy is well beyond the electron spin: there are other concepts worth understanding. EPR spectroscopy monitors the net absorption of energy from a radiation field when molecules change their energy states. Associated with radiation fields are oscillating electric and magnetic fields perpendicular to one another. Like most forms of spectroscopy, it is the magnetic field component that interacts with molecules to cause the change in energy state. The energy absorbed to effect this change is in the form of radiation (usually X-band, microwave energy of 9.36Hz.) quanta (quanta of radiation has energy hν where ν is the frequency of radiation in hertz and h is Planck's constant). Absorption can only occur if two conditions are satisfied:

1. The quanta of radiation (hν) must correspond to the separation (ΔE) of energy levels. When this occurs, resonance condition is said to be met.
2. The oscillating electric (or magnetic) field component of radiation must be able to stimulate an oscillating electric (or magnetic) dipole in the molecule. Once this condition is fulfilled, transition is said to be "allowed"

The magnetic dipoles are provided by electrons and nuclei in the molecule. The electron is of interest as EPR spectroscopy deals primarily with electron magnetic dipoles. Two types of magnetic dipoles are possible: one from the motion of the electron about the nucleus of the atom (orbital magnetic dipole), the other from spinning of the electron about an axis through its centre (spin magnetic dipole). The latter contributes for 99% or more of the total electron magnetic dipole. All electrons have an intrinsic spin that is characterized by a spin angular momentum, P. P and magnetic dipole moment, μ, are always proportional: that is

$$\mu = \gamma P \qquad\qquad (2\text{-}1)$$

where γ is the magnetogyric ratio. It is a unique result of quantum mechanics that the component of P (hence μ) along a given direction can have only two values. If P_z is this component then,

$$L_z = \frac{h}{2\pi} M_s \tag{2-2}$$

where $M_s = \pm\frac{1}{2}$, M_s is called spin quantum number. For classical motion, and, L is the orbital quantum number.

$$\gamma = \frac{-e}{2mc} \tag{2-3}$$

where e is the charge on the electron, m is the mass of the electron and c is the speed of light. A combination of equations (2-1) and (2-3) yields

$$\mu_z = -\frac{eh}{4\pi mc} M_s \tag{2-4}$$

However, spin angular momentum is purely quantum mechanical and cannot be described accurately from classical point of view. Thus,

$$\mu_z = -g\frac{eh}{4\pi mc} M_s = g\beta M_s \tag{2-5}$$

$$\beta = \frac{eh}{4\pi mc} \tag{2-6}$$

(2-6) is called the Bohr magneton and g =2.00232 for a free electron. Also,

$$E = -\mu B \tag{2-7}$$

B is the magnitude of the magnetic field. This implies that

$$E = g\beta B M_s = \pm g\beta B \tag{2-8}$$

This energy is sometimes called the electron Zeeman energy.

Now, if a sample is irradiated with in a certain magnetic field, B, absorption will occur. Therefore, if the energy matches the separation of electron energy levels,

absorption occurs (first condition satisfied). Figure 2.2 shows the splitting of electronic energy levels in the presence of a magnetic field.
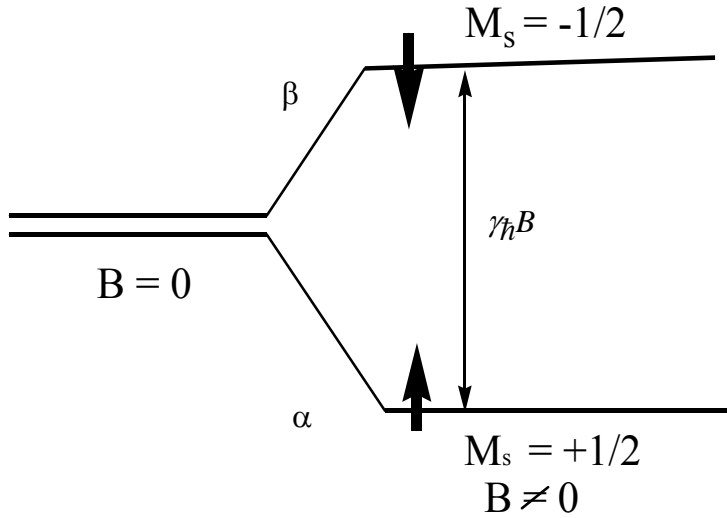
Figure 2. 2: Electronic Energy Levels as a Function of the Magnetic Field Strength.

The second condition is satisfied when the magnetic component of the microwave field is polarized perpendicular to the direction of the static magnetic field. This condition is easily met at the microwave frequency. The energy levels of EPR can be tuned, by varying B to fixed photon energy. For a given microwave frequency, a range of fields will be found at which resonance will occur and, thus, a broad line is generated. The observed line width is defined in terms of the relaxation time, T_2 such that,

$$\Delta B = \frac{\hbar}{g\beta}\left(\frac{1}{T_2}\right)$$
(2-9)

$$\frac{1}{T_2} = \frac{1}{T_2^{'}} + \frac{1}{2T_1}$$
(2-10)

$T_2^{'}$ is called the spin-spin relaxation time and T_2 is a function of the observed line width and T_1 is the spin lattice relaxation time.

Net absorption is a function of the spin population. When resonance is reached, energy is exchanged back and forth between the electromagnetic field and the spin system such that transitions are induced upward and downward in equal proportion. According to the Boltzmann distribution, if there are N^+ electrons in the upper level and N^- in the lower level, with energies E^+ and E^- respectively, then

$$\frac{N^+}{N^-} = EXP\left[\frac{-(E^+ - E^-)}{KT}\right]$$
(2-11a)

Where K is the Boltzmann's constant and T is the absolute temperature. Substitution from equation (2-8) gives

$$\frac{N^+}{N^-} = EXP\left[\frac{-g\beta B}{KT}\right]$$
(2-11b)

$$\frac{N^+}{N^-} \approx 1 - \frac{g\beta B}{KT} = 1 - \frac{h\nu}{KT}$$
(2-11c)

Where,

$$g\beta B << KT$$
(2-11d)

2. 2. The g-factor

The g-factor is related to the ease with which the applied field can 'stir up' current through the molecular framework and the strength of the magnetic field the currents generate. The g-factor therefore gives some information about the molecular structure. The circulation of electrons gives rise to a local magnetic field that may add or subtract from the applied field. The local field strength is proportional to the molecular spin-orbit coupling constant. The g-factor is anisotropic and its magnitude depends on the orientation of the molecule with respect to the applied magnetic field. In solution, when the molecule is tumbling very rapidly, only the average value of the g-factor is observed. Hence, anisotropy of the g-factor is observed only for radicals trapped in solids. The anisotropy of a g-factor is often summarized in the form of a second rank tensor. In a general Cartesian axis system, the g tensor is written as

$$g = \begin{bmatrix} g_{xx} & g_{xy} & g_{xz} \\ g_{yx} & g_{yy} & g_{yz} \\ g_{zx} & g_{zy} & g_{zz} \end{bmatrix}. \qquad (2\text{-}12)$$

The tensor is always symmetric and is defined on a principal axis system x, y, and z in which the g-tensor contain only diagonal elements. That is

$$d_g = \begin{bmatrix} g_{xx} & 0 & 0 \\ 0 & g_{yy} & 0 \\ 0 & 0 & g_{zz} \end{bmatrix} \qquad (2\text{-}13)$$

If the molecule contains a threefold or higher axis of symmetry (z), then x and y are equivalent. The g-factor along z is defined as g_{11} and the other two as $g_{\perp}$. In a broad structureless line, all the information about g-factor is lost, but all possible values of the magnetic field strength would be represented. However, when the g factors differ significantly, the individual values may be obtained even though the system is randomly disordered. This is illustrated for a system with $g_{11} > g_{\perp}$. Figure 2.3 below shows the relative positions of the parallel and perpendicular g-factors on EPR absorption spectra.
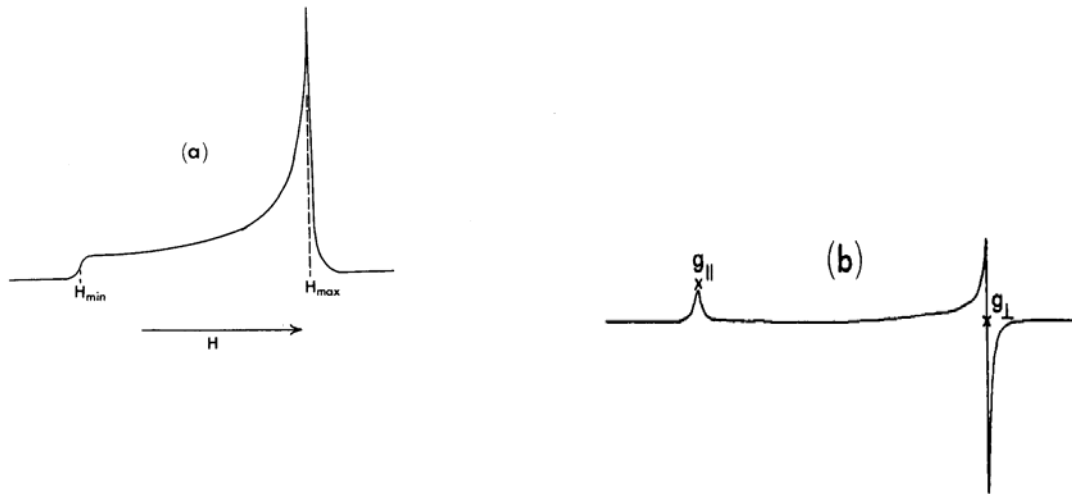
Figure 2. 3: (a) EPR Absorption Spectrum of Symmetric Molecule with No Information about g-factor (b) First Derivative Spectrum. (X's mark the points at which g_{11} and $g_{\perp}$ occurs [18])

$$B_{MIN} = \frac{h\nu}{g_{11}\beta} \qquad (2\text{-}14)$$

$$B_{MAX} = \frac{h\nu}{g_{\perp}\beta} \qquad (2\text{-}15)$$

Where B_{MIN} and B_{MAX} is the minimum and maximum magnetic field strength respectively. The more complicated case of $g_{zz} \neq g_{yy} \neq g_{zz}$ occurs when molecules are randomly oriented. The principal g components can be obtained from spectrum of such molecules as shown on figure 2.4
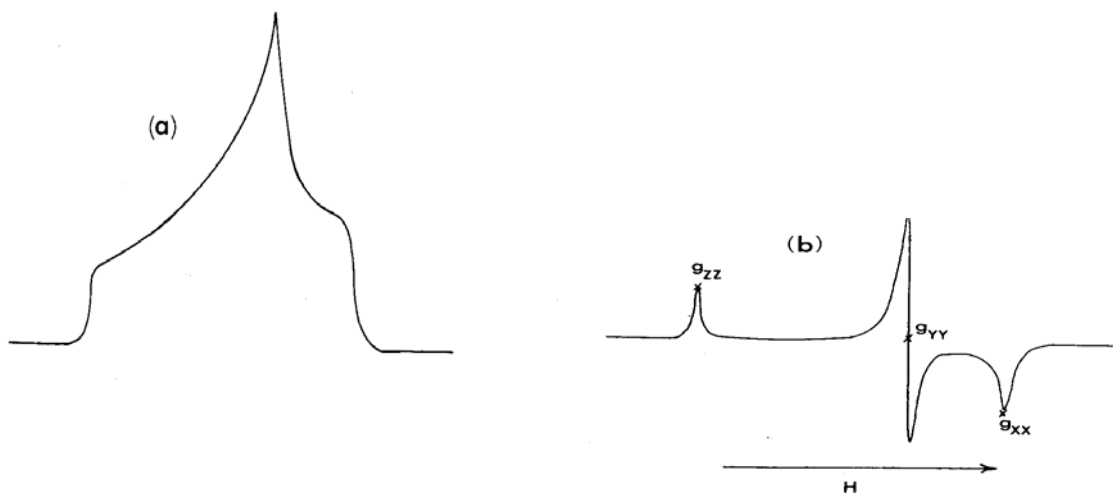
Figure 2. 4: (a) EPR Absorption Spectrum of Irregular Molecules (b) First Derivative Spectrum of Irregular Molecules. (X's mark the point at which g_{xx}, g_{yy}, and g_{zz} occur. By convention, g_{zz} is always the most remote (downfield) g factor and g_{yy} the intermediate [18].)

2. 3. Type of Interaction and Hyperfine Splitting

Besides the local fields induced by the external field that lead to different g factors, there are permanent local fields generated by the presence of other magnetic moments, possibly those of other electrons but more commonly those of magnetic nuclei in the molecule. The interaction of an unpaired electron with a nuclear magnetic moment is termed nuclear hyperfine interaction and is at the origin of the multiple splitting observed in ESR spectra. These lines provide an insight into the detail electronic structure of free radicals. The simplest structure exhibiting hyperfine interaction is the hydrogen atom. Instead of a single line characterized by $H_r = \dfrac{h\nu}{g\beta}$ with g = 2.00232, a pair of lines is observed. This results from the fact that the proton has a spin I = ½. And the corresponding M_I has two allowed values, $\pm 1/2$. There will be two possible values (shown on figure 2.5 below) of external magnetic field at which resonance will occur.

22

100 gauss

3105G   3602G
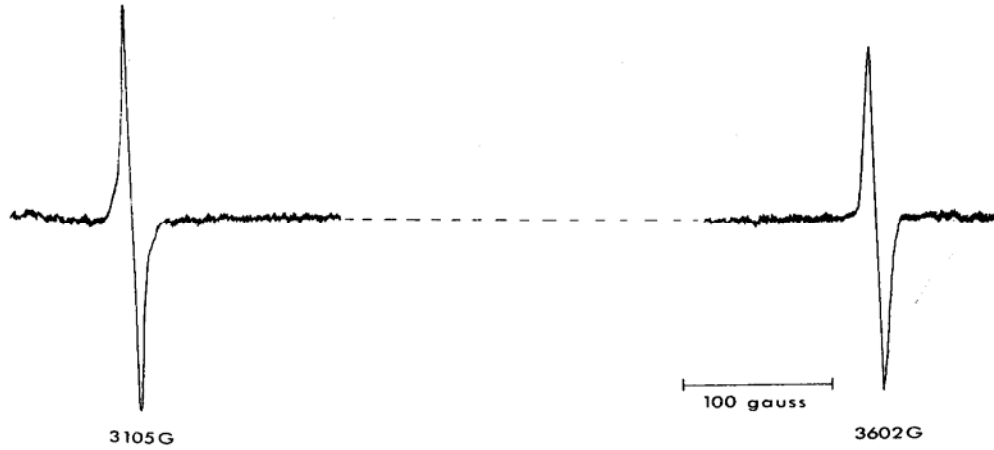
Figure 2. 5**:** EPR Spectrum of H-atom in X rayed Human Tooth [18]

A second type of interaction called hyperfine or Fermi contact interaction arises when the electron has finite probability of being found at the nucleus. This property is only common to electrons in the s-orbital because there is no node in the s-orbital. The value of the hyperfine interaction can be evaluated by using the equation below.

$$\overline{H} = \frac{8\pi}{3} g_e \beta g_N \beta_N |\phi(0)|^2 \overline{S}\,\overline{I} \tag{2-16}$$

from (2-16) the hyperfine splitting constant A_0 can be obtained:

$$A_0 = \frac{8\pi}{3} g_e \beta g_N \beta_N |\phi(0)|^2 \tag{2-17}$$

Where $\phi(0)$ is the value of the wave function of the unpaired electron; g_N and β_N are the nuclear g factor and magneton: $\overline{S}$ and $\overline{I}$ are the electron and nuclear spin operators.

For free radicals in solution of low viscosity, all orientations are made possible by virtue of the rapid molecular tumbling. As such, the isotropic interaction is observed because anisotropy is averaged out by molecular tumbling. If the solution is frozen, the spectrum observed may be a superposition of the spectra from all possible orientations. Figure 2.6 shows the effect of temperature on EPR spectra.
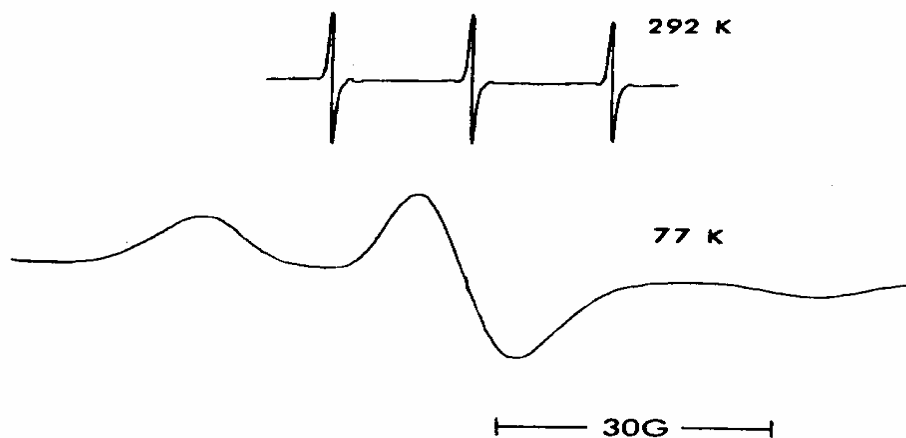
Figure 2.6: First Derivative EPR Spectra of the di-t-butyl Nitroxide Radical (a) in Liquid Ethanol Solution at 292K; (b) in Solid Glass at 77K [18]

The unpaired electron in free radical is often delocalized over many atoms. The electron may be coupled to a number of magnetic nuclei. Two cases are often identified:

1. the electron is coupled to a set of equivalent nuclei
2. the electron is coupled more tightly to one nucleus (or several equivalent nuclei) and less tightly coupled to another.

In the case where an electron is coupled to a set of equivalent nuclei with $I = \frac{1}{2}$, n+1 lines with intensities proportional to the coefficients of the binomial expansion of order n will be observed on the spectrum. On the other hand, for nonequivalent nuclei, the spectrum has to be constructed. The intensities of the peaks are proportional to the number of spin combinations. Obviously, the more nuclei that interact with the unpaired electron, the more complex the EPR spectrum will become.

Aromatic protons, before 1960, were thought to be insensitive to EPR spectroscopy because, in the π-radicals the unpaired electrons are located primarily in the p-orbitals. Also, isotropic hyperfine interaction can be observed only if the unpaired electron has some s-character. In fact, there is an interaction between the π and σ electrons by means of spin polarization mechanism. Hence, proton hyperfine splitting is a sensitive probe of the distribution of unpaired electrons as the relation

24

$$a_i^H = Q\rho_I^\Pi \tag{2-18}$$

has been found to hold reasonably well. Here, a_i^H is the proton hyperfine splitting for a proton adjacent to a carbon atom in a Л system, ρ_i^Π is the fraction of time the unpaired electron spends in the vicinity of the carbon atom i and, Q is a constant (Q~25G)

2. 4. The Schrödinger's Equation

For a long time, the perception of matter at the microscopic level was not evident as the only mathematical model for the study of particles was provided by classical mechanics. Classical mechanics could only provide information on the macroscopic nature of particles. Nowadays, a more refined mathematical model has been designed to solve what used to be poorly understood. This model is called quantum mechanics.

Quantum mechanics attribute dual properties to particles: particle-like as well as wave-like properties. Therefore, from the quantum mechanical prospective, species like protons, electrons, neutrons, etc. have both wave and particle properties. To describe the state of a particle or a system in quantum mechanics a function known as the wave function or state function (ψ) is usually postulated. The way the wave function changes with time is described by the time dependent Schrödinger equation:

$$\frac{-\hbar}{i}\frac{\partial\psi(r,t)}{\partial t} = \left(\frac{-\hbar^2}{2m}\nabla^2 + V(r,t)\right)\psi(r,t) \tag{2-19}$$

In this equation, $\psi(r, t)$ is the wave function in polar coordinates and takes it origin from classical mechanics. The wave function contains all information about a particle, $\hbar$ is a form of Planck's constant, m is the mass of the particle and, ∇^2 is a second order differential operator known as the Laplacian.

$$\nabla^2 = \frac{\partial^2}{\partial x^2} + \frac{\partial^2}{\partial y^2} + \frac{\partial^2}{\partial z^2} \qquad (2\text{-}20)$$

$V(r, t)$ is the potential field in which the particle is moving and is a function of time. Most applications of quantum mechanics to chemistry do not necessitate a time dependent potential field. The wave function can then be written as a product of spatial and time functions.

$$\Psi(r, t) = \psi(r) \, f(t) \qquad (2\text{-}21)$$

Taking partial derivative with respect to time and position, and substituting in (2-19) gives

$$-\frac{\hbar}{i} \frac{1}{f(t)} \frac{df(t)}{dt} = -\frac{\hbar^2}{2m} \frac{1}{\psi(r)} \frac{d^2\psi(r)}{dr^2} + V(r) \qquad (2\text{-}22)$$

Equation (2-22) can be split in to two equations: the left hand side (LHS) is time dependent and the right hand side (RHS) is position dependent. It, therefore, implies that the resulting function must be time and position dependent. So, the LHS and the RHS could be set as equal to energy (E). Equating the RHS to E gives the time-independent Schrödinger equation for a single particle moving in three dimensions

$$\left(-\frac{\hbar^2}{2m} \nabla^2 + V(r) \right) \psi(r) = E\psi(r) \qquad (2\text{-}23)$$

The expression in bracket is the quantum mechanical Hamiltonian operator, H, which, as classically defined, is the sum of the potential energy (V) and the kinetic energy (T) of the particle of interest; V arises from the coulumbic attraction and/or repulsion between charged particles from an isolated system

$$H = T + V \qquad (2\text{-}24)$$

Substituting (2-24) in to (2-23) gives the simple form of the time-independent Schrödinger equation i.e. the eigenvalue equation

$$\hat{H}\psi = E\psi \tag{2-25}$$

An eigenvalue equation produces numerical multiples of the equation known as the eigenvalue. In equation (2-25), ψ is the eigenfunction of the Hamiltonian operator, and E is the eigenvalue.

In a system of particles the kinetic energy is the sum of kinetic energy of all the particles in the system.

$$T = \frac{\hbar^2}{2m_k}\sum_k \nabla^2 \tag{2-26}$$

and the potential energy is the sum of all the coulombic attractions and repulsions between the particles in the system.

$$V = \frac{1}{4\pi\varepsilon_0}\sum_J \sum_{K<j} \frac{q_j q_k}{r_{ij}} \tag{2-27}$$

Where ε_0 is the permittivity of free space, q_j and q_k are the charges on two particles at a distance r_{ij} from each other.

The wave function (ψ) on its own has no physical meaning. For ψ to be meaningful, restrictions are imposed on the particle position so as to determine the wave's intensity that actually is the particles intensity. The intensity of the particle is Schrödinger's interpretation of the wave function: he proposed that a particle's intensity could be given by the expression below:

$$I = \psi(x)^*\psi(x) \tag{2-28}$$

Where I is the intensity and $\psi(x)^*$ and $\psi(x)$ are conjugate and wave functions of a particle respectively. Max Born later found this interpretation difficult as such, he proposed a probabilistic interpretation of the wave function: regarding the intensity or the wave function product as the probability of finding a particle in a volume of space.

Microscopic particles such as electrons, protons, neutrons, photons, and pions have intrinsic (built-in) spin angular momentum that must be taken into account when using wave function to specify their state

$$\psi(r)g(m_s) \tag{2-29}$$

Where $g(m_s)$ is one of the functions, α or β, depending on the value of m_s (-1/2 or 1/2, 1 or -1, 0). The Hamiltonian operator has no effect on the spin function.

$$\hat{H}\left[\psi(r)g(m_s)\right] = E\left[\psi(r)g(m_s)\right] \tag{2-30}$$

Thus, taking spin into account, the energy of the particle is not changed, but there are two possible states ψα and ψβ. Particles with half integral spin, fermions, require symmetric wave functions while particles with integral spins, bosons, require asymmetric wave functions. Thus, we have an additional quantum mechanical postulate, the Pauli principle, which states that the wave function of a system of electrons must be antisymmetric with respect to interchange of any two electrons:

$$\psi(q_1,q_2,,,,q_n) = -\psi(q_1,q_2,,,,,,,q_n) \tag{2-31}$$

The difficulties associated with the separation of variables in solving the many particle Schrödinger's equation suggest the need for approximation. Assuming that the nuclei and electrons are point masses and neglecting spin-orbit and other relativistic interactions, the molecular Hamiltonian is given by the following expression:

$$\overset{\Lambda}{H} = T^{elec}(r) + T^{nul}(R) + V^{nucl-elec}(R,r) + V^{elec}(r) + V^{nucl}(R) \tag{2-32}$$

R and r represent the position of the nuclei and the electron respectively. The Born-Oppenheimer approximation states that the nuclei are much heavier than electrons, because the electrons move faster. This approximation help separate electronic and nuclei motions. Where the purely electronic Hamiltonian is given:

$$\overset{\Lambda}{H} = -\frac{\hbar^2}{2m_\alpha}\sum_i \nabla_i^2 - \sum_\alpha \sum_i \frac{Z_\alpha e'^2}{r_{i\alpha}} + \sum_j \sum_{i>j} \frac{e'^2}{r_{ij}} \tag{2-33}$$

The electronic Hamiltonian including nuclear repulsion is $\overset{\Lambda}{H}_{el} + V_{NN}$. The nuclear repulsion term V_{NN} is given by:

$$V_{NN} = \sum_\alpha \sum_{\beta>\alpha} \frac{Z_\alpha Z_\beta e'^2}{r_{\alpha\beta}} \tag{2-34}$$

The first term in equation (2-13) is the kinetic energy operator for the electron. The second term is the coulombic attraction of the electrons to the nuclei and the third term represent repulsion between electrons. The subscripts i and j represent ith and jth electrons and α represents the αth nuclei. $r_{i\alpha}$ is the distance between the ith electron and the αth nucleus Z_α is the charge on the αth nuclei while r_{ij} is the distance between the ith and the jth electron. Further approximation in solving the Schrödinger's equation for many electrons can be made if model chemistries are employed.

2. 5. Model Chemistries

Model chemistries are approaches in solving the Schrödinger's equation by mathematical approximation: They are the Born-Oppenheimer, the Hartree-Fock Self Consistent (HFSC) theory and, the Density Functional Theory (DFT)

2. 5. 1. Hartree-Fock Self Consistent Field (HF-SCF)

The exact wave function for hydrogen can be calculated while a very accurate wave function can be obtained for helium and lithium. On the other hand, the wave functions of higher atoms can only be obtained if approximations are made. The Hartree-Fock method is the basis for the use of atomic and molecular orbitals in many-electrons system. The Hamiltonian operator for an n-electron atom is given as:

$$\overset{\Lambda}{H} = -\frac{\hbar^2}{2m_e}\sum_{i=1}^{n}\nabla_i^2 - \sum_{i=1}^{n}\frac{Ze'^2}{r_1} + \sum_{i=1}^{n-1}\sum_{j=i+1}^{n}\frac{e'^2}{r_{ij}} \qquad (2\text{-}35)$$

The first term is the sum of kinetic energy for n-electrons. The second term is the potential energy for the attractions between the electrons and the nucleus of charge Ze'

For a neutral atom, $Z = n$, the last term is the potential energy of the interelectronic repulsion; the restriction j>i avoids counting the same interelectronic repulsion twice and avoids terms like $\frac{e'^2}{r_{ii}}$. A zeroth-order wave function can be obtained by neglecting the interelectronic repulsion term. The Schrödinger equation would be separated into n one-hydrogen-like equations. The zeroth-order wave function becomes a product of n hydrogen-like (one-electron) orbital.

$$\psi^{(0)} = f_i(r_1,\theta_1,\phi_2)f_2(r_2,\theta_2,\phi_2),,,,,,,,,,,,,,,,,,f_n(r_n,\theta_n,\phi_n) \qquad (2\text{-}36)$$

Where the hydrogen-like orbitals are:

$$f = R_{n,l}(r)Y_l^m(\theta,\phi) \qquad (2\text{-}37)$$

The approximate wave function (2-36) is qualitatively useful but quantitatively inaccurate as well as all electrons experience the same nuclear charge. The use of effective atomic numbers gives considerable improvement. There is, therefore, the need to set up a variation function that is not restricted to any other particular form of orbitals such as

$$\phi = g_i(r_1, \theta_1, \phi_2) g_2(r_2, \theta_2, \phi_2), , , , , , , , , , , , g_n(r_n, \theta_n, \phi_n) \qquad \text{(2-38a)}$$

The g_i functions that minimizes the variational integral shown below is determined

$$\frac{\int \phi^* \hat{H} \phi dv}{\int \phi^* \phi dv} \qquad \text{(2-38b)}$$

To simplify things, atomic orbitals are product of radial factor and spherical harmonic obtained from approximation:

$$g_i = h_i(r_i) Y_{l_i}^{m}(\theta_i, \phi_i) \qquad \text{(2-39)}$$

This approximation is generally made in atomic calculations. The procedure for calculating g_i's introduced by Hartree in 1928 and is called the Hartree Self-Consistent-field (HSCF) method [24].

2. 5. 1. 1. Hartree's Procedure

Hartree's procedure begins with the guessing of a product wave function.

$$\phi_0 = s_1(r_1, \theta_1, \phi_2) s_2(r_2, \theta_2, \phi_2), , , , , , , , , , , , s_n(r_n, \theta_n, \phi_n) \qquad \text{(2-40)}$$

Where s_1 is the normalized function of r multiplied by a spherical harmonic. Each electron is then considered as interacting with a continuous charge distribution i.e. each electron "sees" the other electrons as being smeared out to form a static distribution of electric charges through which it moves.

Now considering that the charge distribution has a charge density (charge per unit volume) ρ, then the infinitesimal charge in the infinitesimal volume is ρdv. The potential

energy of interaction of any electron carrying a charge Q with the static continuum is given as

$$V = \frac{Q}{4\pi\varepsilon_0} \int \frac{\rho}{r} dv \tag{2-41}$$

r is the distance between Q and ρ. The electrons are ordered such that the first electron has charge Q = e and the second electron is a hypothetical charge cloud given by the equation

$$\rho = -e|s_2|^2 \tag{2-42a}$$

With $|s_2|$, the probability density function of the second electron then is

$$V_{12} = e'^2 \int \frac{|s_2|^2}{r_{12}} dv_2 \tag{2-42b}$$

Where,

$$e'^2 = \frac{e^2}{4\pi\varepsilon_0} \tag{2-42c}$$

Adding the interaction with other electrons we have

$$V_{12} + V_{13} + ,,,,,,,,,,,,,, V_{1n} = \sum_{j=2}^{n} e'^2 \int \frac{|s_j|^2}{r_{1j}} dv_j \tag{2-43}$$

We can adequately approximate that the effective potential acting on an electron is a function of r only. We can, therefore, average $V_1(r_1, \theta_1, \phi_1)$ over the angles to arrive at

$$V_1(r_1) = \frac{\int\limits_{0}^{2\pi}\int\limits_{0}^{\pi} V_1(r_1,\theta_1,\phi_1)Sin\theta_1 d\theta_1 d\phi_1}{\int\limits_{0}^{2\pi}\int\limits_{0}^{\pi} Sin\theta_1 d\theta_1 d\phi_1} \qquad (2\text{-}44)$$

a one electron Schrödinger equation can be written as

$$\left[-\frac{\hbar^2}{2m_e}\nabla_1^2 + V_1(r_1)\right]t_1(1) = \varepsilon_1 t(1) \qquad (2\text{-}45)$$

ε_1 is the energy of the orbital of electron one at this stage and $t_1(1)$ is the improved orbital of electron one. This procedure is repeated for other electrons until improved orbitals are obtained for each electron. The improved orbital calculation is repeated until there is no further change from one iteration to the next. The final sets of orbitals give the Hartree Self-Consistent-Field wave function. The differential equation for finding the Hartree-Fock orbitals has the general form

$$\overset{\Lambda}{F} t_i(i) = \varepsilon_i t_i(i) \qquad (2\text{-}46)$$

$\overset{\Lambda}{F}$ is the Hartree-Fock operator and represents the expression in square bracket in equation (2-45)

In the SCF approximation, the orbital energy is calculated by iteratively solving the one electron Schrödinger equation: the energy of the atom is the sum of the orbital energies minus a correction term. The correction term is the sum of all the potential energies that have been counted twice.

$$E = \sum_{i=1}^{n}\varepsilon_i - \sum_{i=1}^{n-1}\sum_{j-i+1}^{n}\iint\frac{e'^2|g_i(i)|^2|g_j(j)|^2}{r_{ij}}dv_i dv_j \qquad (2\text{-}47)$$

The first summation is the sum of orbital's energies; the second summation is the sum of potential energy terms counted twice.

Although some attention to Pauli principle and spin has been taken, any approximation to the true wave function should include spin explicitly and should be antisymmetric to interchange of electrons. Hence, instead of special orbitals, we must use spin orbitals:

$$\hat{F}\,\mu_i = \varepsilon_i \mu_i \qquad\qquad i = 1, 2, 3\ldots, n \qquad\qquad (2\text{-}48)$$

μ_i is the spin orbital, $\hat{F}$ is the Fock operator and ε_i is the orbital energy of the ith spin-orbital.

The Hartree-Fock method for molecules is basically the same as for atoms. The molecular Hartree-Fock wave function is written as an anti symmetrized product (Slater determinant) of spin orbitals, each spin-orbital being a product of a spatial orbital ϕ_i and a spin function (either α or β).

$$\psi = \frac{1}{\sqrt{N!}}\begin{vmatrix} \phi_1(1)\alpha_1 & \phi_1(1)\beta_1 & - & - & \phi_N(1)\alpha_1 & \phi_N(1)\beta_1 \\ \phi_1(2)\alpha_2 & \phi_1(2)\beta_2 & - & - & \phi_N(2)\alpha_2 & \phi_N(2)\beta_2 \\ - & - & - & - & - & - \\ - & - & - & - & - & - \\ - & - & - & - & - & - \\ \phi_1(N)\alpha_N & \phi_1(N)\beta_N & - & - & \phi_N(N)\alpha_N & \phi_n(N)\beta_N \end{vmatrix} \qquad (2\text{-}49)$$

The expression for the Hartree-Fock molecular electronic energy E_{HF} is given by the variation theorem as shown.

$$E_{HF} = \left\langle \psi \left| \hat{H}_{el} + V_{NN} \right| \psi \right\rangle \qquad\qquad (2\text{-}50)$$

Where ψ is the Slater determinant Hartree-Fock wave function and $\hat{H}_{el}$ and V_{NN} are given by (2-35) and (2-36) respectively. $\hat{H}_{el}$ is the sum of one-electron operators and

two- electron operators. The HF energy of a diatomic or polyatomic molecule with only closed shells is given as

$$E_{HF} = 2\sum_{i=1}^{n/2} H_{ii}^{core} + \sum_{i=1}^{n/2}\sum_{j=1}^{n/2}(2J_{ij} + K_{ij}) + V_{NN} \qquad (2\text{-}51)$$

Where H_{ii}^{core} the one-electron is core Hamiltonian, J_{ij} and K_{ij} are the coulomb and exchange integrals respectively. The HF method looks for those orbitals ϕ_i that minimize the variational integral E_{HF}, also the closed shell orthogonal Hartree-Fock MOs satisfy

$$\hat{F}(1)\phi_i(1) = \varepsilon_i\phi_i(1) \qquad (2\text{-}52)$$

Where ε_i is the orbital energy and $\hat{F}$ is the (Hartree-Fock) operator. Molecular orbital

(MO) calculations are greatly simplified by the orthogonality of MOs. By multiplying (2-34) by ϕ_i and integrating over all space and also using the fact that ϕ_i is normalized we obtain

$$\varepsilon_i = \int \phi(1)\hat{F}(1)\phi_i(1)dv_i \qquad (2\text{-}53)$$

Simplifying 2-35 result in

$$\varepsilon_i = H_i^{core} + \sum_{j=1}^{n/2}(2J_{ij} - K_{ij}) \qquad (2\text{-}54)$$

Finally, solving for $\sum_{i=1}^{n/2} H_{ii}^{core}$ and substituting the result in equation (2-51), the Hartree-Fock energy is obtained.

$$E_{HF} = 2\sum_{i=1}^{n/2}\varepsilon_i - \sum_{i=1}^{n\backslash 2}\sum_{j=1}^{n/2}(2J_{ij} - K_{ij}) + V_{NN} \qquad (2\text{-}55)$$

In 1951 Roothan proposed to expand the spatial orbitals ϕ_i as a linear combination of a set of one electron basis function X_s:

$$\phi_i = \sum_{s=1}^{b} C_{Si} X_s \tag{2-56}$$

Substituting (2-56) in Hartree-Fock equation, we obtain

$$\sum_s C_{si} \overset{\Lambda}{F} X_S = \varepsilon_i \sum_s C_{si} X_s \tag{2-57}$$

Multiplying by X_r and integrating (2-57) gives

$$\sum_{s=1}^{b} C_{si} (F_{rs} - \varepsilon_i S_{rs}) = 0 \quad ; r = 1, 2, , , , , , b \tag{2-58}$$

For a non trivial solution we must have

$$\det(F_{rs} - \varepsilon_i S_{rs}) = 0 \tag{2-59}$$

Equation (2-58) is the (Hartree-Fock) Roothaan equations and must be solved by an iterative process. Because the F_{rs} integrals depend on the orbitals ϕ_i which in turn depend on the unknown coefficients C_{si} in practice, the term SCF wave function is applied to any wave function obtained by iterative solution of Roothaan equations. The HF-SCF method produces the best wave functions that can be expressed as a single Slater determinant. The wave function describes electron-electron repulsion in an average sense but does not include electron correlation. The correlation may be defined as the difference between the exact energy of the system (E_{exact}) and the energy calculated by the HF-SCF theory E_{HF}

$$E_C^{HF} = E_{exact} - E_{HF} \tag{2-60}$$

The exact energy is determined experimentally or in some cases from more accurate calculations. The Hartree-Fock method is available in NWChem by using HF keyword in the root section of the input

2. 6. Density Functional Theory (DFT)

DFT replaces the N-electron wave function and the associated Schrödinger equation by the much simpler electron density and its associated scheme of calculation. The original idea of DFT emanates from the works of Thomas and Fermi in 1927. They proposed that "electrons are distributed uniformly in the six dimensional phase space for the motion of an electron at the rate of two for each h^3 of volume" and that there is an effective potential field that "is itself determined by the nuclear charge and this distribution of electrons." [22]. In the Thomas-Fermi method, the kinetic energy of the system of electrons is approximated as an explicit functional of the density, but neglect exchange and correlation among electrons. Later, the Thomas and Fermi approximation was extended by Dirac, who formulated the local approximation for exchange giving rise to the energy functional for electrons in an external potential

$$E_{TF}[\rho] = E^T[\rho] + E^V[\rho] + E^J[\rho] + E^{XC}[\rho] \qquad (2\text{-}61)$$

E^T is the kinetic energy of the electron, E^V is the external potential energy (nuclei are external to ρ) from electron-nuclear interaction and nuclear-nuclear repulsion, E^J is the electron repulsion term, E^{XC} is the exchange correlation term equivalent to the usual Hartree-Fock energy and representing part of the electron-electron interactions. These electron interactions include the exchange energy, from the antisymmetry of the wave function and the dynamic correlation in the motion of the individual electrons.

The kinetic energy functional of the electron and the electron repulsion functional do not provide a practical way of calculating Hartree-Fock energy functional because they are unknown. On the other hand, the exchange correlation energy functional is

normally written as the sum of exchange functional and correlation functional. The exchange correlation functional is the key to the Kohn-Sham DFT calculation of molecular properties. It is thus necessary to have a good approximation of this term.

The proper approximation of the exchange correlation energy is achieved by explicitly separating out the independent particle kinetic energy and the long-range Hartree terms; $E^{XC}[\rho]$ is reasonably approximated as a local or nearly local functional of the density. Thus, $E^{XC}[\rho]$ is expressed as

$$E^{XC}[\rho] = \int dr \rho(r) \varepsilon^{xc}([\rho], r) \qquad (2\text{-}62)$$

(2-62) implies that $E^{XC}[\rho]$ can be calculated locally at a position r and exclusively from the positional value of ρ. ε^{xc} is the energy per electron at point r that depend only on ρ.

Furthermore, the local density and x_α approximations along with the famous Dirac exchange energy produces the exchange energy of a uniform free electron gas in the following form:

$$E^{X}_{LDA}[\rho] = -\frac{3}{2}\alpha K_D[\rho] = -\frac{9}{8}\alpha\left(\frac{3}{\pi}\right)^{\frac{1}{3}}\int P^{\frac{4}{3}}(r)dr \qquad (2\text{-}63)$$

Where $K_D[\rho]$ is the Dirac exchange-energy formula and α is an empirical constant for the type of system being described and has a value of 2/3 for a uniform free electron gas. However, the use of Local Density Approximation (LDA) exchange still leaves about 10% error in the Hartree-Fock exchange energy [23].

The limitations of the Kohn-Sham Local Density Approximation (KS-LDA) are corrected by the Kohn-Sham Local-Spin-Density Approximation (KS-LSDA). The LDA for exchange energy functional is given by

$$E^{X}_{LSDA}[\rho^\alpha, \rho^\beta] = 2^{\frac{1}{3}}C_X \int \left((\rho^\alpha)^{\frac{4}{3}} + (\rho^\beta)^{\frac{4}{3}}\right)dr \qquad (2\text{-}64)$$

If the spin polarization parameter is defined as

$$\varsigma = \frac{\rho^\alpha - \rho^\beta}{\rho} = \frac{\rho^\alpha - \rho^\beta}{\rho^\alpha + \rho^\beta} \tag{2-65}$$

The exchange energy becomes

$$E_{LSD}^X = \int \rho \varepsilon^x(\rho,\varsigma)dr \tag{2-66}$$

Where,

$$\varepsilon^x(\rho,\varsigma) = \varepsilon_x^0(\rho) + \left[\varepsilon_x^{'}(\rho) - \varepsilon_x^0(\rho)\right]f(\varsigma) \tag{2-67}$$

ς is zero everywhere for an unpolarised system (closed-shell system, B3LYP) and has a value between zero and one for polarized system (open-shell UB3LYP). The spin density ρ is zero for a closed-shell system and one for an open-shell system. The spin is one-half the product of the total spin density ρ and (ς +1) and the β is the difference between the total spin density and the α spin density. The superscript-zero is the exchange energy density for the spin-compensated ("paramagnetic") homogeneous electron gas and the superscript-one is for spin-completely-polarized ("ferromagnetic") homogeneous electron gas.

It has been pointed out that the major source of error in LDA is the exchange energy. So, by imposing the correct exchange hole on the approximate hole given by the gradient expansion, the 10% falls to 1% [24]. This new model has further been simplified to the so called generalized gradient approximation (GGA)

$$E_{GGA}^X[\rho] = \frac{-3}{4}\left(\frac{3}{\pi}\right)^{\frac{1}{3}}\int dr \rho^{\frac{4}{3}} F(s) \tag{2-68}$$

with

$$S = \frac{|\nabla \rho(r)|}{2K_F \rho} \qquad (2\text{-}69)$$

$$K_F = (3\pi^2 \rho)^{\frac{1}{3}} \qquad (2\text{-}70\}$$

and

$$F(s) = (1 + 1.296S^2 + 14S^4 + 0.2S^6)^{\frac{1}{15}} \qquad (2\text{-}71)$$

Much has been done to reduce the error on the exchange correlation energy via the exchange functional. Thus any exchange function can be combined with any correlation functional. For example the B3LYP exchange-correlation functional is a hybrid functional and is written as follows:

$$E_{B3LYP}^{XC} = (1-a)E_{LSDA}^{X} + aE_{HF}^{X} + bE_{B88}^{X} + (1-c)E_{LSDA}^{C} + cE_{LYP}^{C} \qquad (2\text{-}72)$$

This functional incorporates HF and DFT exchange terms. Where B88 and LYP stand for Becke's 1988 exchange functional and Lee-Young-Parr correlation functional respectively.

All in all, the Kohn-Sham theory involves the solving of the following equation

$$F(1)\psi = \varepsilon\psi \qquad (2\text{-}73)$$

Where

$$F(1) = -\frac{1}{2}\nabla_1^2 - \sum_\alpha \frac{Z_\alpha}{r_{1\alpha}} + \sum_j J_j(1) + V^{XC} \qquad (2\text{-}74a)$$

$$V^{XC} = \frac{\partial E^{XC}}{\partial \rho} \qquad (2\text{-}74b)$$

When the Kohn-Sham orbitals (ψ_i) are obtained, the electron density may be obtained from the sum over the occupied orbitals:

$$\rho = \sum_i |\psi_i|^2 \qquad (2\text{-}75)$$

Becke's three-parameter hybrid functional with the Lee-Young-Parr correlation is the best known DFT method.

2. 7. Basis Set

The set of atomic functions used to construct linear combination of atomic orbitals-molecular orbitals (LCAO-MOs) is called basis set. For example $1s_{H_A}$ and $1s_{H_B}$ constitute the basis set for the molecular orbital σ1s the two most common basis sets are Slater-type orbitals and Gaussian-type orbitals. Although the Slater orbitals were used for many years, they are not used directly anymore because the resulting secular determinants are difficult to evaluate. In particular, integrals involving more than one nuclear center, called multicenter integrals are awkward to calculate. This makes their evaluation awkward. Gaussian functions are used instead. For this property study, we used the Gaussian type orbitals. Gaussian-type orbitals are of the form

$$G_{nlm}(r,\theta,\phi) = N_n r^{n-1} e^{-\alpha r^2} Y_l^m(\Theta,\Phi) \qquad (2\text{-}76)$$

The resulting molecular orbitals are linear combinations of atomic orbitals now expressed as sum of Gaussian functions

$$\psi_i = \sum_{i=1}^m C_{ki}\phi_i . \qquad (2\text{-}77)$$

Where m is the number of atomic orbitals used to construct molecular orbitals (i, e the number of basis set). The use of (2-76) and (2-77) does not distinguish one orbital type from the other. A function that adjusts the shape of orbitals is, therefore, needed. This is

done by generating the basis set from two Slater type orbital with different orbital exponent. This is called the double-zeta basis set.

In general, only valence orbitals are expressed by double-zeta representation. The inner-shell electrons are still described by single Slater orbital. Basis sets that describe the inner-shell electron by a single Slater orbital and the valence-shell by a sum of Slater orbitals are commonly referred to as split-valence basis sets. For example 6-31G basis set used on a carbon atom means that the1s orbital (inner-shell orbital) is given by a sum of 6 Gaussian functions. The hyphen indicates a split-valence basis set implying that the valence 2s and 2p orbitals are each represented by a pair of Slater orbitals. One of the Slater orbitals, the smaller one, is represented by a sum of three Gaussian function (hence 3) and the larger orbital is represented by a single Gaussian function (hence 1).

Atomic orbitals distort as atoms are brought together. Such an effect is called a polarization effect. Polarization effects are accounted for by the addition of orbitals of higher orbital quantum number to the mathematical expression of a given orbital e.g. $2p_z$ orbital to 1s hydrogen orbital, 3d-orbital to the 2p orbitals. The addition of 3d-orbitals to 2p orbitals of second row elements of the periodic table is indicated by an asterisk to the basis set. A double asterisk indicates polarization is also being added on hydrogen atoms by adding 2p orbitals to the hydrogen 1s orbitals. An exception to this is the 3-21G* in which the asterisk implies the addition of d-orbitals to the second row atoms. This difference is often marked by writing the asterisk in brackets i.e. 3-21G (*)

The triple-zeta basis set has its valence orbital functions separated into three subsets. A typical example of the triple-zeta is 6-311++G (2d) wherein the inner shell is a linear combination of 6 Gaussian functions, the hyphen indicates a split valence: in this case the inner valence is described by 3 Gaussian functions and the outer valence is described by two separate Gaussian functions. The 2d means that a polarization function has been added to each part of the outer valence shell. One or two plus signs indicate the addition of diffused function with one plus sign indicating the addition of diffuse functions on atoms other than hydrogen atom and two plus signs indicating addition of diffuse functions on all the atoms in the system. Diffused functions are Gaussian orbitals

that have a very small α parameter that allows the wave function to extend far from the nucleus; they are used for describing weakly bound states. Also, when polarization is considered by adding different orbitals, the added orbitals are represented in parenthesis as follows: 6-31G (d, p) means that extra sets of p and d functions have been added to non hydrogen atoms and p extra functions have been added to hydrogens. Thus, this is synonymous with 6-31G**.

Two types of basis sets are commonly used: restricted and unrestricted. The restricted basis sets are used to model closed shell systems while the unrestricted basis sets are used to model open shell systems.

2. 8. Solvent Effect.

To this point, all that has been discussed is on the stationary-state quantum mechanics of an isolated molecule. The molecular properties so calculated are appropriate for gas phase molecules not at high pressure. However, molecules with biological activities are in an aqueous environment.

The most common way to calculate solvent effects is to use a continuum solvent model (COSMO) wherein the molecular structure of the solvent is ignored and the solvent is modeled as a continuous dielectric of infinite extent that surrounds a cavity containing the solute molecule. The continuous dielectric is characterized by its dielectric constant (relative permittivity), ε_r, whose value is the experimental dielectric constant of the solvent at the temperature and pressure of the solution. The solute molecule (M) can be treated in two ways: one, classically as a collection of charges that interact with dielectric. Two, quantum mechanically as the interaction between a solute molecule and the surrounding dielectric continuum modeled by a term, $\overset{\Lambda}{V}_{int}$, that is added to the molecular electronic (fixed nuclei) Hamiltonian $\overset{\Lambda\ (0)}{H}_M$ (for M in a vacuum). To achieve self-consistency between the M charge distribution and the solvent's reaction field in the quantum mechanical implementation of continuum solvation model, the electronic wave function and electronic probability density of the solute molecule, M, are allowed to

change on going from the gas phase to the solution phase. Any treatment in which self-consistency is achieved is called a self-consistent reaction field (SCRF) model. The various versions of SCRF model only differ in how they choose the size and shape of the cavity that contains the solute molecule and how $\hat{V}_{int}$ is calculated.

In NWChem, COSMO is a conductor-like screening model of A. Klamt and G. Schürman. It describes the dielectric screening effects in solvents. COSMO is invoked by specifying the input, COSMO input block with input options followed by the task directive specifying the wave function and type of calculation. The COSMO (conductor-like solvation model) method uses realistic solute-molecule (molecules are modeled to real situation). The charges are conductors, rather than dielectric; the initial charges are then multiplied by the function (ε_r-1) (ε_r+0.5) to yield approximations for the charges suitable for the dielectric solvent.

2. 9. Atomic Units

Most of the results obtained using quantum mechanical calculations are obtained using atomic units. The atomic units system is based on Gaussian units defined as follows: the unit of mass is the electrons mass (m_e), the unit of charge is the proton's charge $e^{'}$, and the unit of angular momentum is $\hbar$. It could be concluded that all constants in quantum mechanical calculation are considered as unity (they are given an arbitrary value of one). Furthermore, the atomic unit of energy $\dfrac{e^{'2}}{a_0}$ is called the Hartree (E_h)

$$E_h = \frac{e^2}{4\pi\varepsilon_0 a_0} = 27.2116 \text{ eV} \qquad (2\text{-}78)$$

a_0 is the Bohr radius. The Bohr is also the atomic unit of length and the unit of permittivity is $4\pi\varepsilon_0$

$$a_0 = \frac{\hbar^2}{m_e e'^2} = 0.5291177 \text{ Å} \tag{2-79}$$

Thus, the use of atomic units save time and memory space

CHAPTER 3

RESULTS AND DISCUSSION

3.1 Computational Details

NWChem 5.0 from Molecular Sciences Laboratory Software Group of Pacific Northwest National Laboratory (MSLSGPNNL) [18-19] and the standard basis set 6-31G* were used to perform geometric optimization and single point energy calculations at the DFT level of theory and the B3LYP [20] exchange correlation functional. The calculations were managed and the pictures generated with ECCE 4.0 from MSLSGPNNL

The calculations were performed on a nine node Fedora Core 4 Linux base computer cluster consisting of a HP DL 145 G2 master node (dual AMD Opteron 246'S 3GB RAM, 160 SATA HDD), seven compute nodes (DL 145, dual Opteron 242'S, 1GB RAM, 40GB PATA HDD) and a file server node (DL 145, dual Opteron 242'S, 2GB RAM~1TB U320 SCSI/SATA RAID 5 drive array). The nodes were connected using a dual switched gigabit Ethernet network.

The hyperfine calculations were performed using Gaussian 98 [26] program on a Dell workstation, model Precision 530 with XEON, duo processor on LINUX 60 professional operating system. The molecular structures were input via Z-matrix of the optimized geometries from NWChem. The EPR properties were computed at the DFT level of theory using the 6-31 (d) and 6-311 (2dp, f) basis sets at the B3LYP exchange correlation functional. The keyword for hyperfine coupling constants (anisotropic) in Gaussian 98 is Prop, which is specified in the root section. The root section of Gaussian 98 job is initiated by a pound sign (#) as the first non blank character of a line.

The dielectric effect was computed by performing self-consistent reaction field (SCRF) calculations using the Polarized Continuum Model PCM [25] with the integral equation formalism (SCRF = IEFPCM). The dielectric effect was due to the solvent (water) continuum on tesserae with average area of 0.55 squared angstroms. In the PCM

framework, the solute molecules are embedded in cavities. The cavities are made up of tesserae (small spheres). These cavities are surrounded by water molecules, in the form of a continuum, whose polarization is reproduced by point charges distributed on the cavity surface. The cavities were computed at the DFT level of theory using the 6-31(d) basis and the B3LYP exchange correlation functional with the molecule optimized in the PCM cavity, hyperfine calculations were then carried out on the solvated molecules

The structures of the systems were specified with Z-matrices including Cartesian coordinates. The Cartesian coordinate reference frame work shown below displays the relationships between the input data and the definition of centers and angles, the number of centers being defined are labeled with the respect to C (the first center consider).
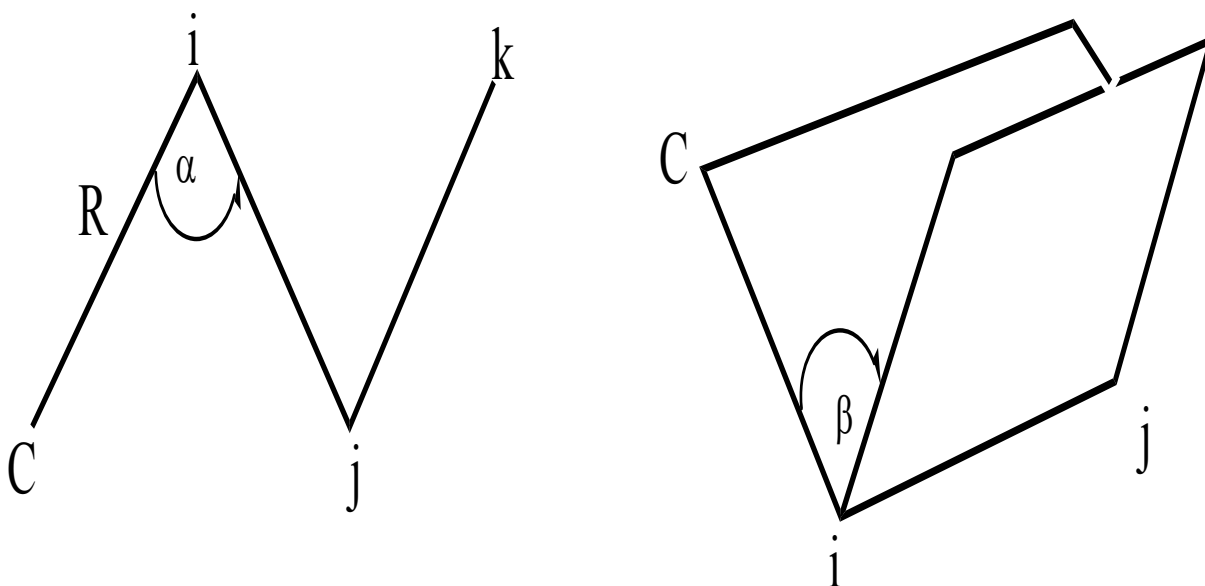
Figure 3.1:Relationships between the Centers Bond Angle and the Dihedral Angle in Z-matrix Input. i, j and k are the Successive Centers from C. (The symbols β and α are the dihedral (tortional) and bond angles respectively.)

Input Line: C i R j alpha k beta +1
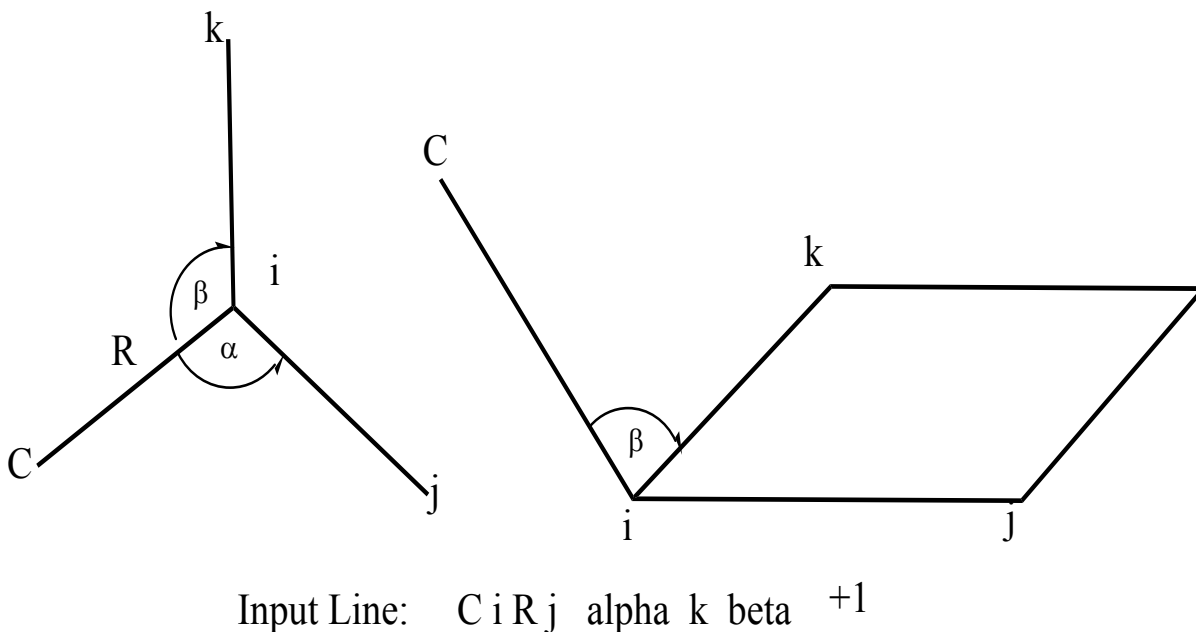
Figure 3. 2: Relationships between the Centers and Two Bond Angles in Z-matrix Input
with Optional Parameter Specified as +1.

Input Line: C i R j alpha k beta -1
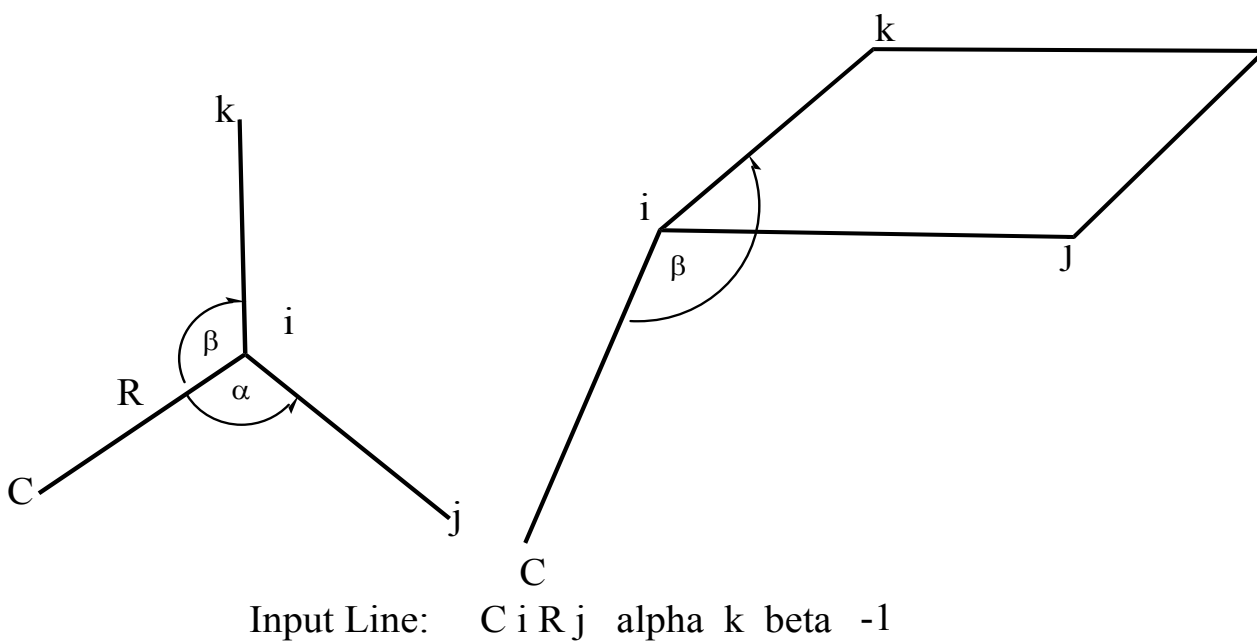
Figure 3.3: Relationships between the Centers and Two Bond Angles in Z-matrix Input
with Optional Parameter Specified as -1.

The input line in the diagrams above describes the geometric relationship among the centers considered: the centers C and i are separated by a distance R (bond length), α is the bond angle between the bond lengths Ci and ij and β is the dihedral angle between the plane defined by Cij and the bond length ik. +1 and -1 optional parameters are defined with respect to the origin of the reference frame.

3.2 Input Files

The input files with the Z-matrices of spin traps and hydroxyl radical based on the referential fore mentioned were generated for each system. The input file gives all the information about the job that is about to be "launched". In NWChem, the input files always start with the job title and proceeds to indicate the symmetry, overall charge, the z-matrix in Cartesian coordinate, the basis set library, the model chemistry and the task to be carried out. The input file is made up of strings, each string describing a specific task. The model chemistry string is one in which key words are quite often added.

Table 3.1: NWChem input file of PBN spin trap

```
Title "PBN"

Start PTBN

echo

charge 0

geometry autosym units angstrom
 C      0.0132390      1.41548      1.23447e-07

 C     -1.26288       0.672114     1.14930e-07

 C     -1.25919      -0.800800     8.15835e-08

 C      0.0206479     -1.53148     -3.41716e-08

 C      1.30339       -0.794713    -2.15101e-07

 C      1.32201        0.702811     1.98769e-08
```

```
H      -0.0198805       2.50068        1.36395e-07

H      -2.20441         1.21106        1.06111e-07

H      -2.19673        -1.34661        8.16780e-08

H       0.0204492      -2.61649       -1.10218e-07

H       2.19319        -1.40205       -7.71507e-07

C       2.54469         1.56620       -1.85923e-07

H       2.35140         2.63432       -5.27706e-07

N       3.78577         1.15727        1.57228e-07

C       4.91316         2.13071        3.06445e-08

C       4.85636         3.01608        1.26457

H       4.83476         2.38093        2.17608

H       5.74519         3.68149        1.31927

H       3.95517         3.66362        1.26917

C       6.27125         1.38923        8.77383e-08

H       6.36614         0.747167       0.902357

H       6.36614         0.747167      -0.902356

H       7.11823         2.10951       -2.60190e-08

C       4.85636         3.01608       -1.26457

H       4.83476         2.38093       -2.17608

H       3.95517         3.66362       -1.26917

H       5.74519         3.68149       -1.31927

O       4.06741        -0.147396       1.09847e-06

end
```

```
ecce_print /home/jacob/nwchem_run/PTBN/ecce.out

basis "ao basis" cartesian print

  H library "6-31G*"

  O library "6-31G*"

  C library "6-31G*"

  N library "6-31G*"

END

dft

  mult 1

  XC b3lyp

  mulliken

end

driver

  default

  maxiter 58

end

task dft optimize
```

3. 3.1 Geometry Analysis

The naming system used in this study is shown in Table 3.2 below.

Table 3.2: Chemical Nomenclature of Systems Studied.

Acronym	Formal Name
HMPO	2- methyl pyrrolidinium-N- oxide
HMPO-OH	5-methyl 2-hydroxyl pyrrolidine-N-oxide
DMPO	2,2 dimethyl pyrrolidinium-N-oxide
DMPO-OH	2,2-dimethyl 5-hydroxylpyrrolidine-N-oxide
PPN	Benzylidene –N-isopropyl-N-oxide
PPN-OH	Hydroxyl(phenyl) methyl-isopropylaminium-N-oxide
PBN	Benzylidene –N, N-tert-butyl oxide
PBN-OH	Hydroxyl (phenyl)methyl-t-butylaminium-N-oxide

The spin traps studied are classified into two groups: DMPO-type and PBN-type. The structure in each case has distinct characteristics. The calculated N-O and C=N bond lengths in both spin traps and spin adducts of the DMPO-types are in the range 1.26-1.28 and 1.30-1.31Å [14a] which agrees with those determined by Frederick A. Villamena et al while the C-N bond length is in the range of 1.27-1.49Å in the spin trap as well as spin adducts of the DMPO-types. Also, the O-H bond length in both DMPO-OH and HMPO-OH adducts are in the range 0.97-0.98Å which is close to the 0.96Å O-H bond length of water. The C13-C9-N11 and C16-C12-N10 angles in both HMPO and DMPO respectively, are in the range 106.54-111.59˚. Also, the dihedral angle, C13-C9-N11-O12 drops by 48% in the spin adduct HMPO-OH. The same kind of drop in dihedral angle of 14% is observed in DMPO-OH spin adduct. This is explained to some extent by the loss of the double bond. The double bond contributes to the rigidity of the ring in the DMPO-

type spin traps. Figures 3.4 and 3.5 are the optimized geometries of DMPO and PBN parent spin traps and the daughter DMPO and PBN hydroxyl adduct radicals.

Unlike the DMPO-type nitrone where the main skeleton is a ring, the PBN-type nitrone has as principal frame, a methyl to which the substituents are attached. The feature marks are C=N bond which is 1.32Å in both PBN and PPN spin traps. The C-N bond in the spin trap as well as the adduct for both PPN and PBN nitrones is in the range of 1.46-1.54Å. Furthermore, the N-O bond is in the range 1.27-1.28Å that agrees with the range obtained in DMPO-type as well as the literature. The O-H bond does not change much as from the DMPO-type. Table 3.3 compares the calculated bond lengths to the experimental bond lengths obtained from X-ray scattering.

Table 3.3: Comparison of Calculated (DFT/B3LYP/6-31G*) Bond Lengths with Experimental Bond Lengths

Bond	Calculated range(Å)	Experimental(Å) [14]
C=N	1.30-1.31	1.291-1.307
C-N	1.49-1.54	1.50
N-O	1.26-1.28	1.27
O-H	0.97-0.98	1.02
$C_{ph} - C_N$	1.45-1.51	N/A

.
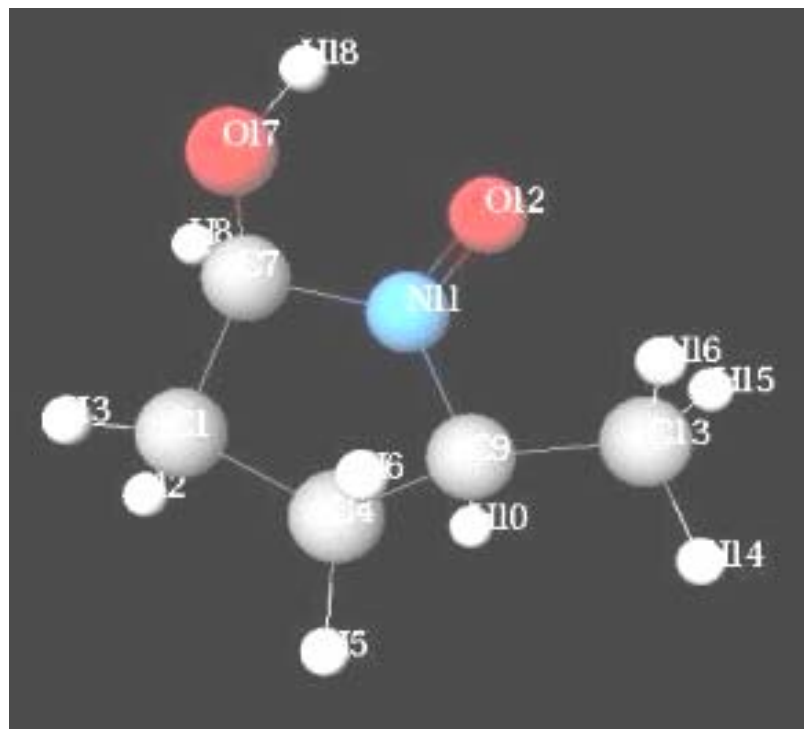
(a)
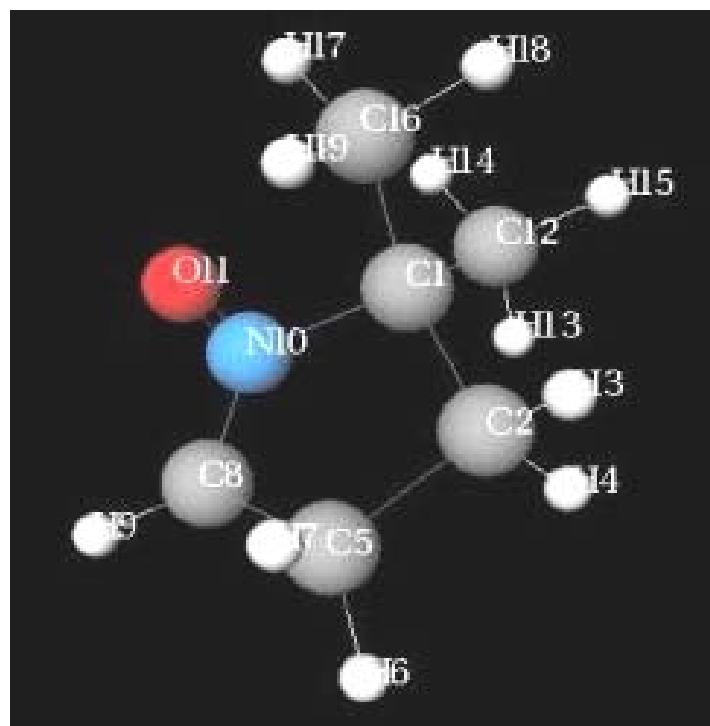
(b)

Figure3.4: NWChem Optimized Geometries of (a) DMPH-OH and (b) DMPO Spin Traps.
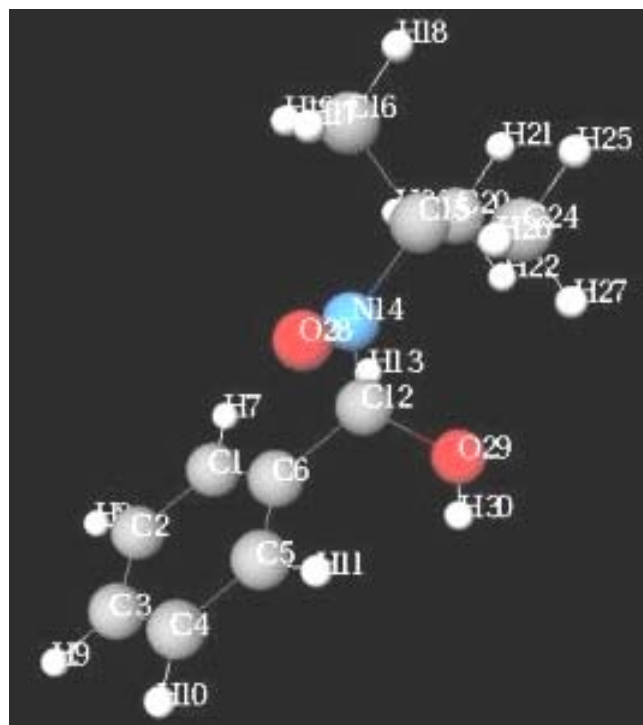
(a)
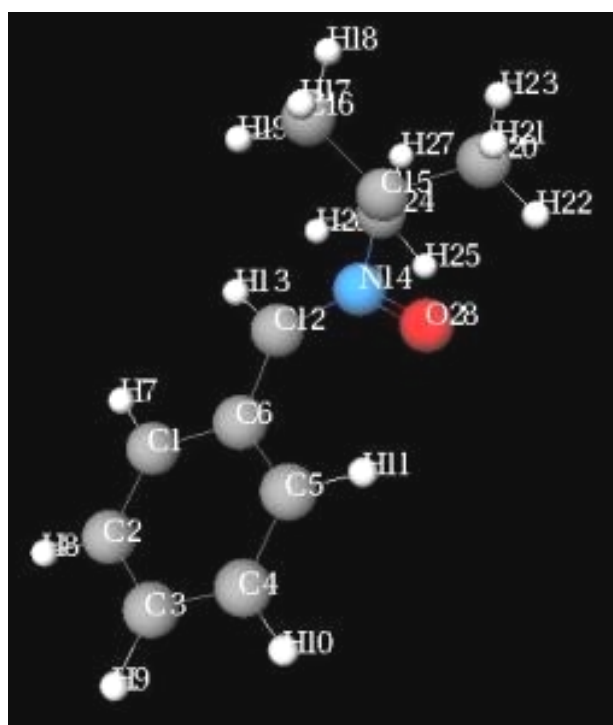
(b)

Figure 3.5: NWChem Optimized Geometries of (a) PBN-OH and (b) PBN Spin Traps.

The molecular energies of both spin traps and adducts (Table 3.4 below) are indicative of the fact that both the DMPO-type and PBN-type are exoergic with the DMPO-type being more exoergic. Also the adduct formed are more exoergic than the spin traps. This difference in exoergicity implies that the adduct formed are more stable than the parent spin traps. The fact that the adduct of the DMPO-type nitrone is more stable than that of the PBN-type might be responsible for the selectivity of the PBN-type nitrone. It might be important to note the fact that the adducts as well as the spin traps increase in stability as the number of atoms in the molecule are decreased. Likewise, the stabilization energy decreases as the number of atoms in the molecular skeleton increases. Tables 3.4 and 3.5 show the molecular energies as well as the stabilization energies of the parent spin traps and the daughter hydroxyl radical adduct as well as the hydroxyl adduct radical respectively.

Table 3.4: Molecular Energies of DMPO and PBN Spin Traps and Adducts at the B3LYP/6-31G* Level

Molecule	Molecular Energy*/ E_h
OH	-75.69
HMPO-OH	-401.68
HMPO	-325.86
DMPO	-365.18
DMPO-OH	-440.99
PPN-OH	-594.61
PPN	-518.81
PBN-OH	-633.92
PBN	-558.12

*All table energies are in hartrees and 1 hartree is 2625.500 kJ/mol

Table 3.5: Molecular Stabilization Energies of the Hydroxyl Radical Adducts at the
B3LYP/6-31G* Level

Molecules	Stabilization Energy*/ E_h
PPN-OH	-0.111
PBN-OH	-0.115
DMPH-OH	-0.130
DMPO-OH	-0.131

*Spin trap + hydroxyl radical – radical adduct

Table 3.4 shows the molecular energies of the DMPO and PBN spin traps and
hydroxyl radicals, while the adduct stabilization energies are shown in Table 3.5. From
the table of values the radical adducts formed are about -0.12 hartrees (-315 kJ/mol) more
stable than the parent spin trap and free radical. This is in agreement with previous
studies made by Dr. Frederick A. Villamena et al. [14]. Also, the difference in
stabilization energy between the two types of spin traps is relatively small 0.01 to 0.02
hartrees which is about 26.2 to 52.5 kJ/mol.

3.3.2 Solvent Effects

Considering the fact that biological probes are generally active in biological
media, it is wise to carry out a solvent effect study on the spin traps as well as the
adducts. This is a strong motivation to determine the effect of the solvent on the molecule
relative to the gaseous phase. This was investigated using the polarizable continuum
model (PCM). Slight changes in molecular parameters are expected upon solvation: the
structures are expected to relax to permit greater charge separation (electronic

polarization), the solute also is expected to polarize the solvent (electric polarization). The molecular free energy in solution can be written as

$$G_{PCM} = G_{es} + G_{cav} + G_{dis-rep}$$

(3-1)

where G is the free energy and the subscripts stand for electrostatic, cavitations and dispersion-repulsion respectively. The electrostatic contribution gives an account of the various kinds of interaction as shown by the expression.

$$G_{ES} =< Ph > +1/2 < PG > +V_{NN} +1/2(U_{NN})$$

(3-2)

P is the solute density matrix; h and G are the density matrix for isolated solute V_{NN} is the solute nuclear repulsion energy and U_{NN} describes the solute-solvent interaction in terms of the polarization charges.

Table 3.6: Electrostatic Free Energies of DMPO-type and PBN-type Spin Traps at the B3LYP/6-31G* Level

Molecules	G_{es} (kcal/mol)
PPN	-5.99
PBN	-5.19
DMPH	-8.40
DMPO	-8.70

Table 3.7: Electrostatic Free Energies of DMPO-type and PBN-type Hydroxyl Radicals at the B3LYP/6-31G* Level

Molecules	G_{es} (Kcal/mol)
PPN-OH	-9.26
PBN-OH	-8.96
DMPH-OH	-6.43
DMPO-OH	-6.14

From Table 3.6, the values of the energies reveals the strengths of both intermolecular and intramolecular interactions that follow the trend PPN-OH > PBN-OH > DMPH-OH > DMPO-OH for the adduct hydroxyl radicals, and DMPH > DMPO >PPN >PBN for the spin traps. It is also evident from these values that DMPO and DMPH spin traps are the more interactive electrostatically in aqueous medium both intermolecular and intramolecular-wise than their hydroxyl radical adduct with DMPO being less interactive than DMPH, though not very significant. Furthermore, free energy differences between the PBN-type and DMPO-type are in the range 3.51-3.21 kcal/mol which gives the DMPO-type, an interactive edge over the PBN-type. However, PBN-type hydroxyl radicals show a higher degree of interaction with an interactive free energy of about -2.82 kcal/mol more than that of the DMPO-type hydroxyl radicals as shown by the values in Table 3.7 above. Thus, as a whole, solvation will perturb the relative energy of the molecules very slightly as a result of the high exothermicity of the molecule in the gaseous phase. There is, thus, an agreement with the findings of Frederick A. Villamena *et al.* [14] in their kinetic study of alkoxycarbonyl and dialkoxyphosphoryl nitrones in aqueous media in which they found out using the PCM model that the solvation energy of a number of molecules, spin traps an adduct radicals, was in a range from -0.77 to 1.50 kcal/mol, which is very small compare to the energies of the molecules.

The cavity energy is expressed as the sum over the spheres forming the cavity. i.e.

$$G_{cav} = \sum_{spheres} \frac{A_i}{4\pi R_i^2} G_i^{HS}$$

(3-3)

where R_i is the radius of the ith sphere and G_i^{HS} is the cavitation energy for the sphere. There is actually no interaction between the solute atoms and the cavities. The absence of interaction is from the fact that the solute atoms are embedded in the cavities. As such, the whole combination is considered as an entity thus, G_i^{HS} has a value of zero and consequently, G_{CAV} is also zero.

The dispersion-repulsion term contributes between 61% and 81% to the PCM free energy for both the PBN-type and the DMPO-type spin trap and adduct hydroxyl radicals alike. However, this term for the PBN-type nitrones is smaller than the DMPO-type nitrones. From Tables 3.8 and 3.9, the dispersion-repulsion energy increase in the order DMPH > DMPO >PPN >PBN for the spin trap and in the order DMPH-OH > DMPO-OH > PPN-OH > PBN-OH for the adduct hydroxyl radical. The PCM free energy follows the same trend.

Table 3.8: Dispersion-repulsion Free Energy of DMPO-type and PBN-type Spin Traps at the B3LYP/6-31G* Level

Molecules	$G_{dis-rep}$	G_{PCM}
PPN	-21.07	-27.06
PBN	-22.34	-27.53
DMPO	-15.35	-23.75
DMPH	-13.96	-22.66

Note: All energy terms are in kcal/mol

Table 3.9: Dispersion-repulsion Free Energy of DMPO-type and PBN-type Hydroxyl Radical Adducts

Molecules	$G_{dis-rep}$	G_{PCM}
PPN-OH	-21.56	-30.82
PBN-OH	-22.79	-31.75
DMPO-OH	-16.50	-22.64
DMPH-OH	-15.09	-21.52

Note: All energy terms are in kcal/mol

From the trend of the PCM cavity free energy, as shown by table 3.9, the solvent-solute interaction is consistently exothermic with the PBN-type and their hydroxyl radical adduct being the more exothermic. Further, confirmation of the trend is shown by the calculated dipoles moments as seen from tables 3.10 and 3.11. The higher the dipole moment the more exothermic the species. Nonetheless, our calculated values dipoles (DMPO, DMPO-OH types) do not agree with those calculated by Frederick A. Villamena *et al.*, though the same models (PCM), same basis set (6-31G (d)) and the same correlation functional (B3LYP) were used.

Table 3.10: Dipole moments of DMPO-type and PBN-type Spin Traps at the B3LYP/6-31G* Level

Molecules	Calculated dipole moment(D)	Literature values [14b]
PPN	4.08	n/a
PBN	4.20	n/a
DMPO	5.34	3.72
DMPH	5.37	4.03

Table 3.11: Dipole Moments of DMPO-type and PBN-type Hydroxyl Radical Adducts at the B3LYP/6-31G* Level

Molecules	Calculated dipole moment(D)	Literature values [14b]
PPN-OH	4.01	n/a
PBN-OH	4.48	n/a
DMPO-OH	3.57	2.5
DMPH-OH	2.76	2.23

Note: The dipole moment values in table 3.10 and 3.11 are in Debye (D).

Finally, the solvation energies of the PBN and DMPO spin traps are constant for each type with the DMPO-type having relatively higher solvation energy (52.52 kJ/mol higher). The high exothermicity of the solvation of the PBN-type spin traps suggest they are less stable in solution than their DMPO-type counter parts. Table 3.12 gives the solvation energies (the difference between PCM energy and gas phase molecular energy) of both spin traps and adducts of DMPO-type and PBN-type nitrones. It is worth mentioning that the solvation of the spin trap is very important for efficient spin trapping activities.

Table 3.12: Calculated Solvation Energies of DMPO-type and PBN-type Nitrones in Water at the B3LYP/6-31G* Level

Molecule	Solvation Energy	Molecule	Solvation Energy
PPN-OH	-0.05	PPN	-0.05
PBN-OH	-0.05	PBN	-0.05
DMPO-OH	-0.04	DMPO	-0.03
DMPH-OH	-018	DMPH	-0.03

The energies are in hartree (1hartree = 2625.500 kJ/mol)

Table 3.13: Free Energies of PBN-type and DMPO-type Nitrones with Non-Electrostatic Interactions at the B3LYP/6-31G* Level

Molecule	Free Energy	Molecule	Free Energy
PPN-OH	-594.66	PPN	-518.86
PBN-OH	-633.97	PBN	-558.17
DMPO-OH	-441.03	DMPO	-365.21
DMPH-OH	-401.85	DMPH	-325.89

Energies are in hartree (1hartree =2625.500 kJ/mol)

On the other hand, hydroxyl adducts radicals of DMPO-type nitrones are more stable in solution than the hydroxyl radical adduct of the PBN-type nitrones. This stability of the hydroxyl radical is very essential in the concentration build up for EPR identification. Table 3.13 shows the free energy of the nitrones with non-electrostatic terms i.e. terms that do not involve electrostatic interaction: solute-solute, solute-solvent and solvent-solvent interactions.

3.3.3 Hyperfine Properties

A close look at the spin density distribution on various hydroxyl adduct radicals using natural population analyses reveals the delocalized nature of spin density over all the molecular orbitals. In gaseous as well as in aqueous media, the spin densities are highly concentrated on the nitrogen nuclei in the range between 40% and 48%. It can be seen that in the DMPO hydroxyl radical adduct, at least 1 γ -H exhibits a 0.2% spin density distribution while several β-H's spin density distribution can be predicted between 0.8% and 3.0%.

Also, it is worth remarking that 95% of the spin density distribution is on the nitrogen and terminal oxygen nuclei. Figure 3.6 below shows the spin density distribution on the DMPO hydroxyl radical adduct.
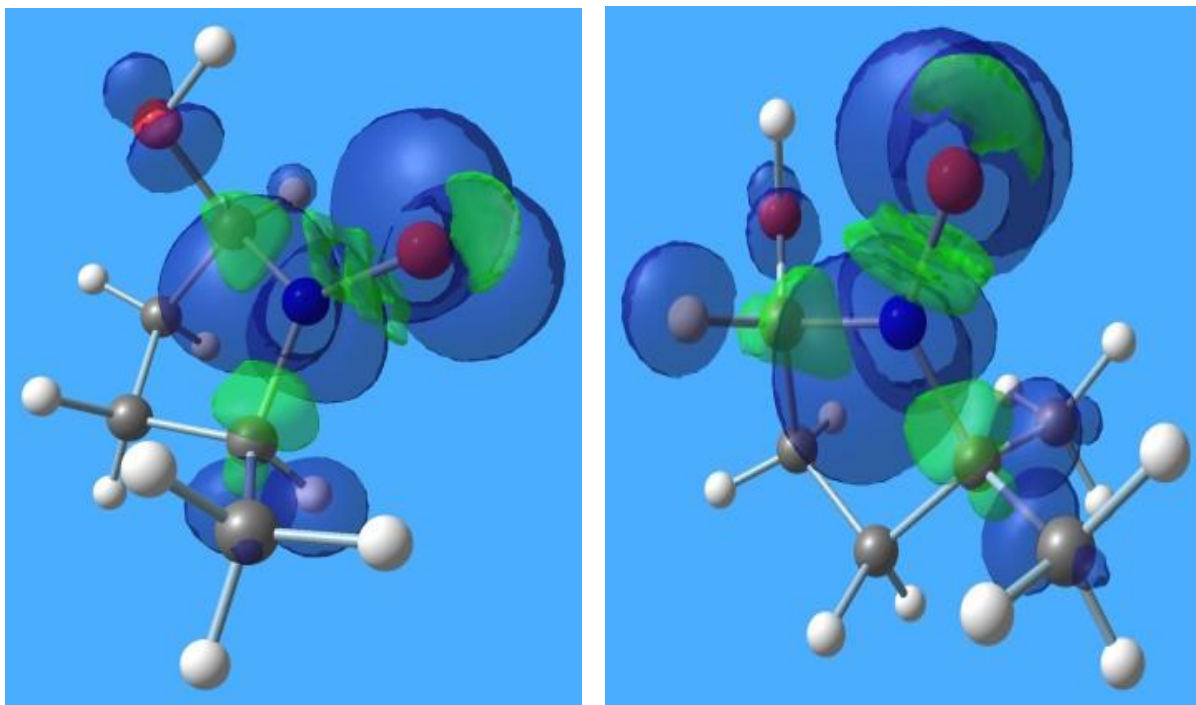
Figure3.6: Gaussian View Spin Density Distribution of DMPO Hydroxyl Radical Adducts (HMPO-OH and DMPO-OH respectively).

The PBN hydroxyl radical adducts show a different spin density distribution. A 0.65%-0.74% spin density distribution is noticeable on the hydroxyl hydrogen. Furthermore, as in the case of DMPO hydroxyl radical adduct, 96% spin density distribution is on nitrogen and the terminal oxygen. Figures 3.7 and 3.8 are the density distribution maps of the PBN and PPN hydroxyl radicals. Unlike the high spin density distribution on oxygen and the terminal oxygen, very low spin density is determined on the benzene ring.
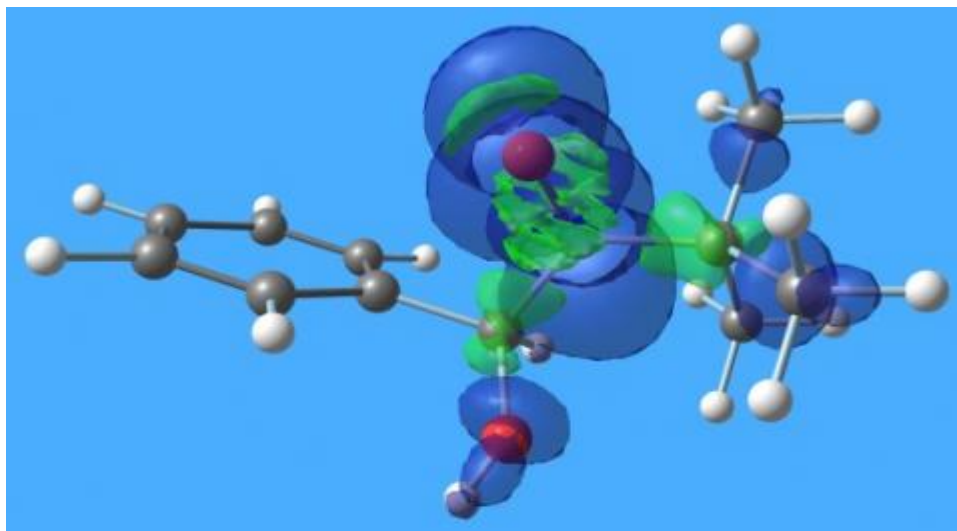
Figure3.7: Gaussian View Spin Density Distribution Map of the PBN-OH Radical
Adduct.
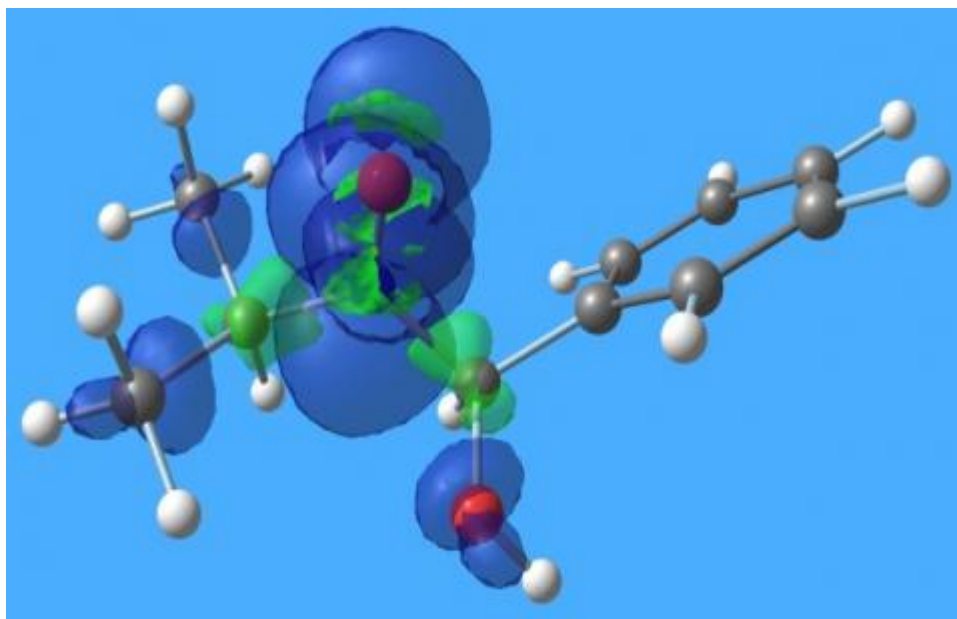
Figure 3.8: Gaussian View spin density distribution map of the PBN-OH radical adduct.

The green color in figures 3.7 and 3.8 indicates the spin density while the blue
color represents the atomic orbital. Having obtained the values of spin densities on the
various nuclei, the values of the isotropic hyperfine coupling constant, a_x, for the various
adducts can be calculated using the expression

$$a_x = \frac{2\mu_0}{3}\left(\frac{g}{g_e}\right)g_n\beta_n\left|\rho_{(0)}\right|^2$$

<div align="right">(3-4)</div>

where g_e, is the g-value for the free electron, β_n is the nuclear Bohr magneton, $\rho_{(0)}$ is the nuclear spin density, g_n is the nuclear g-factor, μ_0 is the magnetic dipole. From the table 3.14 below, the spin density distributions, in gaseous phase, on the hydrogen atoms seem very insignificant; however, the small spin density distribution gives rise to large hyperfine splitting constants.

Table 3.14: Significant Spin Densities and Hyperfine Splitting Constants of the DMPO and PBN Hydroxyl Radicals at the DFT, 6-31G (d)/6-311G (2df, p)/B3LYP Level

Molecule	Atoms	ρ 6-31G(d)	a_x(G) 6-31G(d)	ρ 6-311G(2df,p)	a_x(G) 6-311G(2df,p)
PBN-OH	H13	0.0017	2.43	0.0026	2.54
	H30	0.0074	3.75	0.0077	3.51
	N14	0.4100	12.77	0.4000	10.18
PPN-OH	N14	0.4090	12.50	0.3988	9.91
	H26	0.0065	3.42	0.0067	3.21
DMPO-OH	H9	0.0222	16.12	0.0220	16.15
	N10	0.4524	12.99	0.4410	10.11
	H15	0.0021	1.80	0.0020	1.83
HMPO-OH	H8	0.0118	6.65	0.0110	6.80
	H10	0.0297	21.12	0.0310	21.03
	N11	0.4347	11.60	0.4310	9.01

ρ = spin density, a_x = hyperfine coupling constant.

There is a great difference between the hyperfine splitting constants of PBN Hydroxyl adduct and DMPO hydroxyl radicals. The hyperfine splitting constants of DMPO hydroxyl radicals are 3-10 times larger than that of PBN adducts

The hyperfine properties determined in both cases, gaseous and aqueous media, showed no significant difference. The values of the hyperfine splitting constants and spin densities in aqueous as well as in gaseous phases were very close to each other. Table 3.15 shows the hyperfine splitting constant in aqueous environment.

Table 3.15: Spin Densities and the Hyperfine Splitting Constants of PBN-type and DMPO-type Adducts

Molecule	Atoms	ρ 6-31G(d)	a_x (MHz) 6-31G(d)
PBN-OH	H13	0.0025	2.97
	H30	0.0057	3.15
	N14	0.443	13.15
PPN-OH	N14	0.4400	13.28
	H26	0.0055	3.36
DMPO-OH	H9	0.023	16.81
	N10	0.475	13.58
	H15	0.0022	1.91
HMPO-OH	H8	0.0140	6.60
	H10	0.0350	22.41
	N11	0.4550	10.73

Furthermore, as suggested by the solvation energies and the free energies as well as the solution energies, the hydroxyl radical adduct of DMPO nitrones-type are more stable in solution than the hydroxyl radical adducts of the PBN-type nitrones. This stability of the hydroxyl radical is essential in the concentration build up for EPR

identification. The literature value [16] of the hyperfine splitting constant of the nitrogen and beta hydrogen in DMPO-OH (14.90 G and 14.9 G respectively) calculated at the HF/6-31G* level differ by 12.8% and 8.2% respectively from the calculated value in the gaseous phase.

3.3.4 EPR Spectra

EPR spectroscopy is the most commonly used technique in spin trap characterization. The spin traps are considered to be powdery; data from hyperfine coupling was used in the input file.
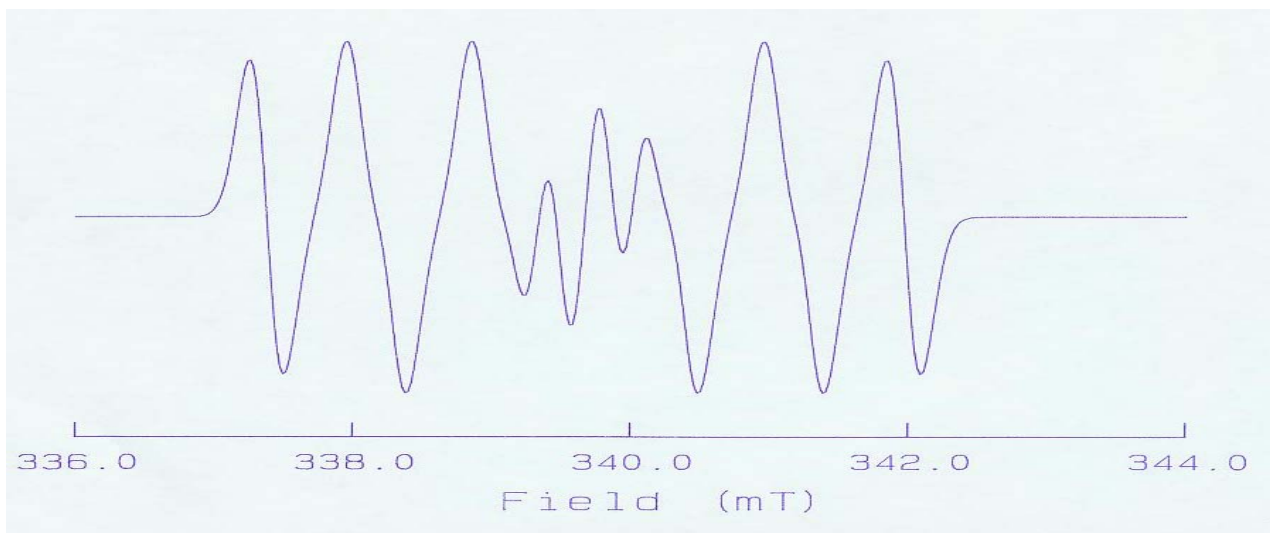
Figure 3.9: Simulated EPR spectrum of DMPO-OH.
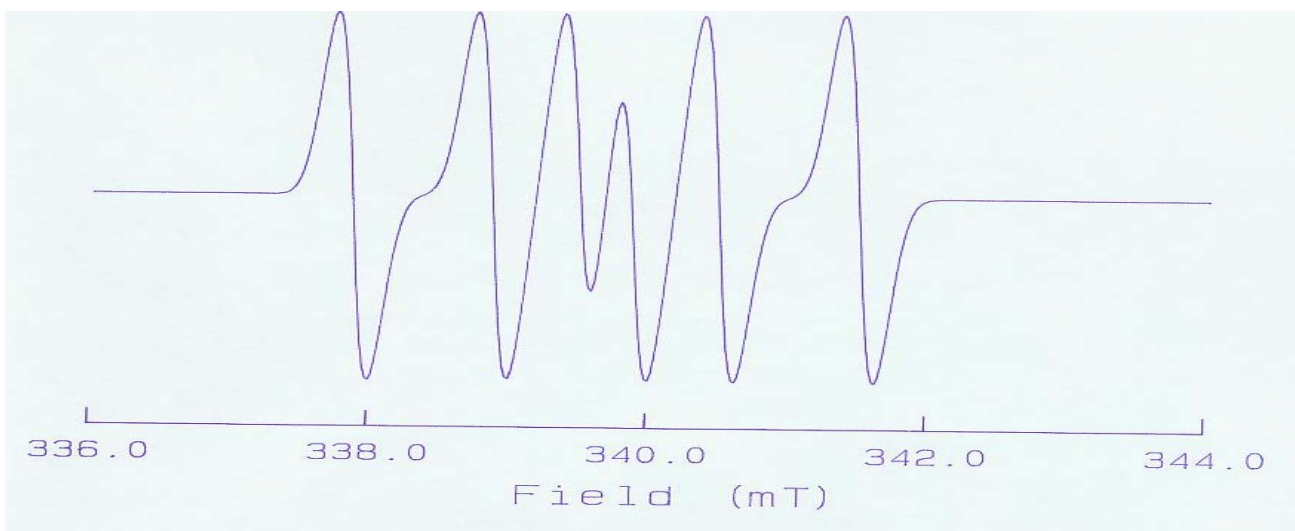
Figure 10: Simulated EPR spectrum of DMPH-OH.
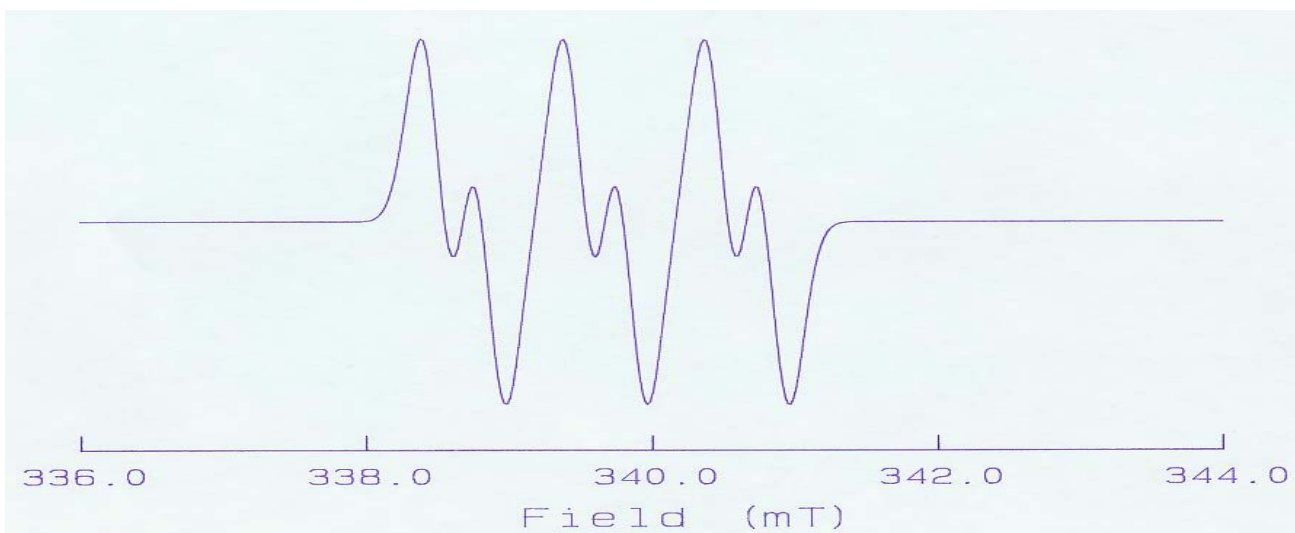
Figure 11: Simulated EPR spectrum of PPN-OH.
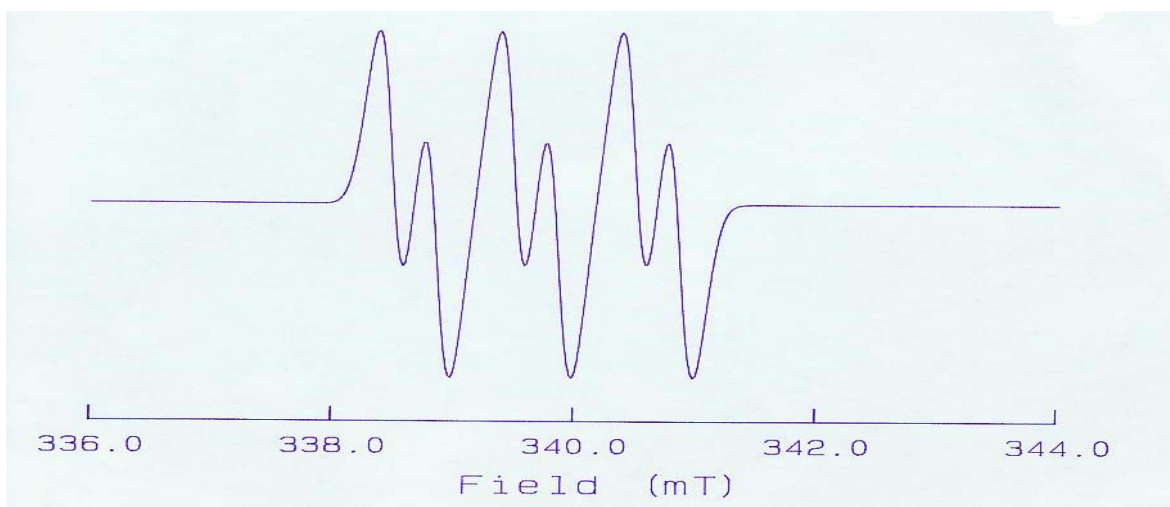
Figure 12: Simulated EPR Spectrum of PBN-OH.

The DMPO-OH adduct is very distinguishable by the nature of its splitting that is due to H9 and N14. The rigid ring reinforces the interaction between hydrogen and nitrogen. The DMPH-OH has a spectrum that is very similar to that of the DMPO-OH but for the fact that the interaction is mainly between N14 and H10 where as the N14, H8 interaction, is of longer range. The PPN-OH and PBN-OH adduct spectra are not very distinguishable from each other. The nature of interaction between N and H with significant spin constant is dependent on the relative distance between N14 and H26 in PPN-OH and between N14 and H13 in PBN-OH. Thus, the relative extent of the split peak on the PBN-OH spectra is due to the proximity of H13 to N14.

Summary of Results and Future Work

The radical adducts formed are about 0.12 hartree (-315kJ/mol) more stable than the parent spin trap and free radical. Also, the DMPO spin trap types form relatively more stable adducts comparatively to the PBN spin trap types. The difference in stabilization energy between the two types of spin traps is relatively small 0.01-0.02 hartree which is about 26.2 and 52.5 KJ/mol

The value of the electrostatic free energies reveals the strength of both intermolecular and intramolecular interactions. The trend is in the order PPN-OH > PBN-OH > DMPH-OH > DMPO-OH for the adduct hydroxyl radicals, and DMPH > DMPO >PPN >PBN for the spin traps. It is also evident from these values that DMPO and DMPH spin traps are the more interactive both intermolecular and intramolecular than their hydroxyl adduct radical adduct with DMPO being less interactive than DMPH, though not very significant.

The solvation energies of the PBN and DMPO spin traps are constant for each type with the DMPO-type having relatively higher solvation energy (52.52 kJ/mol higher).

Furthermore, as suggested by the solvation energies and the electrostatic free energies as well as the solution energies, the hydroxyl radical adduct of DMPO nitrones-type are more stable in solution than the hydroxyl radical adducts of the PBN-type nitrones.

In gaseous as well as in aqueous media, the spin densities are highly concentrated on nitrogen nuclei in the range between 40% and 48%. In DMPO hydroxyl radical adduct, at least 1γ-H exhibit a 0.2% spin density distribution while several β-H's spin density distribution can be predicted between 0.8% and 3.0%. Also, it is worth remarking that 95% of the spin density distribution is on the nitrogen and terminal oxygen nuclei.

The future work to be done would be to determine the effects of electrophilic and electrophobic substituents on spin density distribution on the molecular orbital. Also, the solvent effect could be studied with water molecules in the PCM cavity.

BIBLIOGRAPHY

1. http://www.sircuitskin.com/spin_trap, 04/20/06

2. G. K. Fraenkel, J. M. Hirshon and C. Walling, J. Am. Chem. Soc. (1954) 76, 3606

3. Acken, B. J. ; Gallis, D. E.; Warshaw, J. A.; Crist, D. R. Can. J. Chem. 1992, 70, 2076-2080.

4. Gallis, D. E.; Warshaw, J. A.; Acken, B. J.; Crist, D. R. Collect. Czech. Chem. Commun. 1993, 59, 125-41.

5. Zeghdaoui, A; Tuccio, B.; Finet, J-P.; Cerri, V.; Tordo, P. J. Chem. Soc., Perkin Trans. 2 1995, 12, 2087-2089.

6. Frejaville, C.; Karoui, H.; Tuccio, B.; Le Moigne, F.; Culcasi, M.; Pietri, S.; Lauricella, R.; Tordo, P. J. Med. Chem. 1995, 38, 258-265.

7. Lui, K. J.; Miyake, M.; Panz, T.; Swartz, H. Free Radical Biol. Med.1999, 26, 714-721.

8. Stolze, K; Udilova, N.; Nohl, H. Free Radical Biol. Med 2000, 29, 1005-1014.

9. Chalier, F.; Tordo, P. J. Chem. Soc., Perkin Trans. 2002, 2, 2110-2117.

10. Olive, G.J Mercier, A.; Le Moigne, F.; Rockenbauer, A. ; Tordo, P. Free Radical Biol. Med. 2000, 28, 403-408.

11. Zhang, H.; Joseph, J.; Vasquez-vivar, J ; Karoui, H.; Nsanzumushire, C.; Martasek, P. ; Tordo, P.; Kalyanaraman, B. FEBS Lett. 2000, 473, 58-62

12. Stolze, K.; Udilova, N; Nohl, H. Biol. Chem. 2002, 383, 813-820

13. Stolze, K.; Udilova, N.; Rosenau, T.; Hofinger, A.Nohl, H. Biol. Chem. 2003, 384, 493-500

14. Frederick A.Villamena et al. J. Org. Chem, 2004, 69, 7994-8004

15. Frederick A.Villamena et al. J. Phys. Chem. Vol. 107, No. 22, 2003

16. Frederick A.Villamena et al. J. Phys. Chem. A 2003, 107, 4407-4414

17. Milos Mojovic, Ivan Spasojevic, and Goran Bacic. J. Chem. Inf. Model. 2005, 45, 1716-1718.

18. Harold M. Swartz; James R. Bolton; Donald C. Borg; Biological Applications of Electron Spin Resonance, John Wiley & Sons, Inc., 1-36, 1972.

19. Makino, K.; Mossoba, M. M.; Reisz, P. J. Phys. Chem. 1983, 87, 1369-1377.

20. Apra, E.; Windus, TL; Stratsma, T P.; et al; NWChem, A computational Chemistry package for parallel computers. Version 5. 0" 2006 PNN Richland Washington 99352-0999, USA.

21. Kendal, R. A; Apra, E; Bernholdt, D. E; et al; Computer phys. Comm. 2000, 128, 260-283.

22. Parr R. G., Yang, W; Density Functional Theory of Atoms and Molecules, Oxford New York, 185-187, 1989.

23. Parr R. G., Yang, W; Density Functional Theory of Atoms and Molecules, Oxford New York, 47-51, 1989.

24. Parr R. G., Yang, W; Density Functional Theory of Atoms and Molecules, Oxford New York, 197-200, 1989.

25. Becke, A. D; J. Chem. Phys. 1993, 98, 5648-5652

26. Lee. C; Yang W.; Parr, R.G.; Phys. Rev. B 1998, 37, 785-789

27. "Extensible Computational Chemistry Environment (ECCE), a problem solving environment for computational chemistry, software version 3. 2. 4'(2005), as developed and distributed by PNNL, P. O. Box 999, Richland, Washington 99352, USA and founded by the U. S. Department of Energy, was used to obtain some of these results.

28. Black, G.; Didier, B.; Elsethangen T.; et al "Ecce, A Problem Solving Environment for Computational Chemistry, software version 4.0, PNNL, Richland, Washington 99352-O999, USA"

29. S. M. Blinder, Am. J. Phys., 33, 431(1965).

30. Barone, V.; Cossi, M.; Tomasi, J. J. Chem. Phys. 1997, 107, 3210

31. Frish, M. J.; Trucks,G.W.; Schelegel, H. B.; Suseria, G.E.; Robb, M.A.; Cheeseman, J. R.; Zakrzewski, V.G.; Montgomery, J. A., Jr.; Stratman, R.E.; Burant, J. C. Dapprich, S.; Millam, J. M.; Daniels, A.D.; Kudin, K. N.; Strain, M. C.; Farkas, O.; Tomasi, J.; Borone, V.; Cossi, M.; Cammi, R.; Mennucci, B.; Pomelli, C.; Clifford, S.; Ochterski, J.; Peterson, G. A. Ayala, P.Y.; Cui, Q.; Morokuma, K.; Malick, D. K.; Rebuck, A. D.; Raghavachari, K.; Foresman, J. B.; Cioslowski, J.; Ortiz, J. V.; Baboul, A. G.; Stefanov, B. B.; Lui, G.; Liashenko, A.; Piskorz, P.; Komaromi, I.; Gomperts, R.; Martin, R. L.; Fox, D. J.; Keith, T.; Allaham, M. A.; Peng, C.Y.; Nanayakkara, A.; Challacombe, M.; Gill, P. M. W.; Johnson, B.; Chen, W.; Wong, M. W.; Andres, J. L.; Gonzalez, C.; Head-Gordon, M.; Replogle, E. S.; Pople, J. A. Gaussian 98, Revision A. 11; Gaussian: Pittsburgh, PA, 1998.

APPENDIX A: Structural Details of PBN/PBN-OH

Cartesian coordinates of PBN-OH with DFT/B3LYP/6-31G*

Title "PTBN"		
Start PTBN		
echo		
charge 0		
geometry autosym units angstrom		
C 0.0132390	1.41548	1.23447e-07
C -1.26288	0.672114	1.14930e-07
C -1.25919	-0.800800	8.15835e-08
C 0.0206479	-1.53148	-3.41716e-08
C 1.30339	-0.794713	-2.15101e-07
C 1.32201	0.702811	1.98769e-08
H -0.0198805	2.50068	1.36395e-07
H -2.20441	1.21106	1.06111e-07
H -2.19673	-1.34661	8.16780e-08
H 0.0204492	-2.61649	-1.10218e-07
H 2.19319	-1.40205	-7.71507e-07
C 2.54469	1.56620	-1.85923e-07
H 2.35140	2.63432	-5.27706e-07
N 3.78577	1.15727	1.57228e-07
C 4.91316	2.13071	3.06445e-08
C 4.85636	3.01608	1.26457
H 4.83476	2.38093	2.17608
H 5.74519	3.68149	1.31927
H 3.95517	3.66362	1.26917
C 6.27125	1.38923	8.77383e-08
H 6.36614	0.747167	0.902357

```
 H    6.36614    0.747167    -0.902356
 H    7.11823    2.10951    -2.60190e-08
 C    4.85636    3.01608    -1.26457
 H    4.83476    2.38093    -2.17608
 H    3.95517    3.66362    -1.26917
 H    5.74519    3.68149    -1.31927
 O    4.06741    -0.147396    1.09847e-06
end

ecce_print
/home/jacob/nwchem_run/PTBN/ecce.out

basis "ao basis" cartesian print
  H library "6-31G*"
  O library "6-31G*"
  C library "6-31G*"
  N library "6-31G*"
END

dft
  mult 1
  XC b3lyp
  mulliken
end

driver
  default
  maxiter 58
end

task dft optimize
```

Cartesian coordinates of PBN-OH with DFT/B3LYP/6-31G*

#b3lyp/6-31G(d) scf=tight prop=epr			
1/38=1/1;			
2/17=6,18=5,40=1/2;			
3/5=1,6=6,7=1,11=2,25=1,30=1/1,2,3;			
4//1;			
5/5=2,32=2,38=4,42=-5/2;			
6/7=2,8=2,9=2,10=2,17=2,26=4,28=1/1,2;			
99/5=1,9=1/99;			
pbn-oh opt			

Symbolic Z-matrix:			
Charge = 0 Multiplicity = 2			
C	0.46573	2.02825	1.20585
C	0.0572	3.35955	1.30589
C	-0.48171	4.00606	0.19328
C	-0.61206	3.31749	-1.01611
C	-0.20816	1.98739	-1.11408
C	0.33367	1.33369	-0.00003
H	0.89029	1.52625	2.07292
H	0.16549	3.89007	2.24807
H	-0.79732	5.04353	0.26591
H	-1.03497	3.81769	-1.88328
H	-0.31446	1.44302	-2.04579
C	0.80441	-0.10205	-0.09672
H	1.42957	-0.32847	0.77441
N	-0.31262	-1.0568	-0.07596
C	-0.10399	-2.53208	0.14628
C	-1.31825	-3.03422	0.94478
H	-2.24352	-2.78664	0.42027
H	-1.26023	-4.12083	1.06982
H	-1.3501	-2.57309	1.93835

C	1.18933 -2.79468 0.92936
H	1.28428 -3.87258 1.09755
H	2.07412 -2.46579 0.37568
H	1.17755 -2.30873 1.91184
C	-0.04306 -3.21631 -1.23302
H	0.03565 -4.30286 -1.11251
H	-0.95042 -2.99015 -1.79944
H	0.82002 -2.85975 -1.80216
O	-1.39604 -0.71947 -0.67521
O	1.53873 -0.35707 -1.29777
H	2.18223 0.36369 -1.39936

Isotropic Fermi Contact Couplings for PBN-OH at DFT/B3LYP/6-31G*

Isotropic Fermi Contact Couplings				
Atom	a.u.	MegaHertz	Gauss	10(-4) cm-1
1 C(13)	-0.00043	-0.48503	-0.17307	-0.16179
2 C(13)	0.00005	0.05123	0.01828	0.01709
3 C(13)	-0.00006	-0.06302	-0.02249	-0.02102
4 C(13)	0.00000	0.00500	0.00178	0.00167
5 C(13)	-0.00039	-0.44238	-0.15785	-0.14756
6 C(13)	0.00141	1.58090	0.56410	0.52733
7 H	0.00004	0.15668	0.05591	0.05226
8 H	-0.00001	-0.02577	-0.00919	-0.00859
9 H	0.00001	0.03230	0.01153	0.01077
10 H	0.00002	0.09347	0.03335	0.03118
11 H	-0.00001	-0.03844	-0.01372	-0.01282
12 C(13)	0.00161	1.80747	0.64495	0.60291
13 H	0.00152	6.81106	2.43036	2.27193
14 N(14)	0.11077	35.78918	12.77047	11.93798
15 C(13)	-0.00807	-9.07537	-3.23832	-3.02722
16 C(13)	0.00764	8.58735	3.06418	2.86443
17 H	-0.00024	-1.06256	-0.37915	-0.35443
18 H	-0.00026	-1.14871	-0.40989	-0.38317

19 H	-0.00024	-1.05742	-0.37731	-0.35272	
20 C(13)	-0.00023	-0.25463	-0.09086	-0.08493	
21 H	-0.00036	-1.61632	-0.57674	-0.53915	
22 H	-0.00008	-0.37689	-0.13448	-0.12572	
23 H	-0.00007	-0.32944	-0.11755	-0.10989	
24 C(13)	0.01118	12.57152	4.48583	4.19341	
25 H	0.00053	2.36272	0.84308	0.78812	
26 H	-0.00048	-2.13345	-0.76127	-0.71164	
27 H	-0.00033	-1.45777	-0.52017	-0.48626	
28 O(17)	0.07929	-48.06776	-17.15178	-16.03368	
29 O(17)	0.06057	-36.72131	-13.10308	-12.24891	
30 H	0.00235	10.52251	3.75469	3.50993	

PCM structure for PBN-OH at theDFT/B3LYP/6-31G*

#b3lyp/6-31G(d) scrf=(iefpcm,read) scf=tight geom=checkpoint prop=epr
----
1/29=2,38=1,46=1/1;
2/40=1/2;
3/5=1,6=6,7=1,11=2,25=1,30=1/1,2,3;
4//1;
5/5=2,32=2,38=4,40=2200,42=-5,53=1,54=100/2;
6/7=2,8=2,9=2,10=2,17=2,26=4,28=1/1,2;
99/5=1,9=1/99;
----
pbn-oh opt

Redundant internal coordinates taken from checkpoint file:
ptbn-oh.chk
Charge = 0 Multiplicity = 2
C,0,0.3555984471,1.9921004708,1.28179437

C,0,-0.0737746563,3.314613175,1.4165834562
C,0,-0.5292375933,4.0166098529,0.2988498156
C,0,-0.5526070702,3.3914000485,-0.9517664261
C,0,-0.1271318059,2.0696276092,-1.0833019834
C,0,0.3276852572,1.3597937866,0.0343671952
H,0,0.7191397386,1.4511911541,2.1525803579
H,0,-0.0435782197,3.7962395356,2.3899765156
H,0,-0.8584856874,5.0472359207,0.399123567
H,0,-0.9024520156,3.9355418763,-1.8248817583
H,0,-0.1341877012,1.5815896914,-2.0516644514
C,0,0.809351594,-0.0740211673,-0.0936511579
H,0,1.4640474032,-0.3017126783,0.7530811339
N,0,-0.3102363912,-1.0305020576,-0.033909456
C,0,-0.1082900905,-2.5024882587,0.2234149945
C,0,-1.2937023103,-2.9732227003,1.0825244681
H,0,-2.2399416202,-2.7442293589,0.5873029993
H,0,-1.231805758,-4.0549061095,1.2388407077
H,0,-1.2853332397,-2.4832878767,2.0621187921
C,0,1.2110254779,-2.7563942099,0.9637675322
H,0,1.3021297955,-3.8303408387,1.1545827489
H,0,2.0766451341,-2.4494185077,0.3695285377
H,0,1.2411479003,-2.2456289266,1.9322828664
C,0,-0.1071381155,-3.227768207,-1.135550713
H,0,-0.0232751257,-4.309200625,-0.9839087384
H,0,-1.0376269279,-3.0217133495,-1.6714105128
H,0,0.7331351547,-2.8922385665,-1.7495617503
O,0,-1.4102489662,-0.6948088949,-0.6062909233
O,0,1.4897193447,-0.3257452389,-1.3200712228
H,0,2.2856580736,0.2373237347,-1.3319169643

Cartesian coordinates of PPN with DFT/B3LYP/6-31G*

Title "PPN"			
Start PPN			
echo			
charge 0			
geometry autosym units angstrom			
C	-0.174000	1.38900	0.00000
C	-1.29000	0.544000	0.00000
C	-1.11600	-0.845000	0.00000
C	0.174000	-1.38900	0.00000
C	1.29000	-0.544000	0.00000
C	1.11600	0.845000	0.00000
H	-0.312000	2.48400	0.00000
H	-2.30600	0.973000	0.00000
H	-1.99500	-1.51100	0.00000
H	0.311000	-2.48400	0.00000
H	2.30600	-0.973000	0.00000
C	2.34397	1.77435	3.93267e-17
H	2.19897	2.93533	-3.03975e-08
N	3.74437	1.18335	3.94908e-08
O	3.92779	-0.285242	1.19259e-07
C	4.95639	2.10063	-2.94226e-09
H	4.93453	2.77577	-0.955301
C	4.92761	2.98928	1.25740
H	4.94948	2.31414	2.21271
H	5.86055	3.69535	1.25740
H	3.95095	3.63351	1.25740
C	6.24191	1.25267	8.22754e-08
H	6.26378	0.577525	0.955301

```
 H    6.26378    0.577525    -0.955301
 H    7.17485    1.95874    4.88643e-08
end

ecce_print
/home/jacob/nwchem_run/Spin_trap/PBNH-
1/ecce.out

basis "ao basis" cartesian print
  H library "6-31G*"
  O library "6-31G*"
  C library "6-31G*"
  N library "6-31G*"
END

dft
  mult 1
  XC b3lyp
  mulliken
end

driver
  default
  maxiter 30
end

task dft optimize
```

Isotropic Fermi Contact Couplings for PPN-OH at DFT/B3LYP/6-31G*

	Isotropic Fermi Contact Couplings				
Atom	a.u.	MegaHertz	Gauss	10(-4) cm-1	
1 C(13)	-0.00039	-0.43726	-0.15603	-0.14585	
2 C(13)	0.00004	0.05018	0.01791	0.01674	
3 C(13)	-0.00008	-0.09080	-0.03240	-0.03029	
4 C(13)	0.00007	0.08186	0.02921	0.02731	
5 C(13)	-0.00029	-0.32773	-0.11694	-0.10932	
6 C(13)	0.00144	1.61323	0.57564	0.53812	
7 H	0.00003	0.13769	0.04913	0.04593	
8 H	-0.00001	-0.03462	-0.01235	-0.01155	
9 H	0.00001	0.04691	0.01674	0.01565	
10 H	0.00001	0.05047	0.01801	0.01683	
11 H	0.00000	0.00445	0.00159	0.00149	
12 C(13)	0.00011	0.11950	0.04264	0.03986	
13 H	0.00187	8.33937	2.97569	2.78171	
14 N(14)	0.11405	36.84987	13.14895	12.29179	
15 C(13)	-0.00878	-9.86769	-3.52104	-3.29151	
16 C(13)	0.00829	9.31692	3.32451	3.10779	
17 H	-0.00026	-1.15850	-0.41338	-0.38643	
18 H	-0.00022	-0.99687	-0.35571	-0.33252	
19 H	-0.00025	-1.13868	-0.40631	-0.37982	
20 C(13)	-0.00016	-0.18527	-0.06611	-0.06180	
21 H	-0.00038	-1.71286	-0.61119	-0.57135	
22 H	-0.00009	-0.41180	-0.14694	-0.13736	
23 H	-0.00007	-0.32290	-0.11522	-0.10771	
24 C(13)	0.01179	13.25296	4.72899	4.42071	
25 H	0.00053	2.36897	0.84531	0.79020	
26 H	-0.00049	-2.19353	-0.78271	-0.73168	
27 H	-0.00036	-1.59798	-0.57020	-0.53303	
28 O(17)	0.07650	-46.37742	-16.54862	-15.46984	
29 O(17)	0.05462	-33.11015	-11.81453	-11.04436	
30 H	0.00197	8.82752	3.14988	2.94455	

PCM structure for PPN-OH at theDFT/B3LYP/6-31G*

#b3lyp/6-31G(d) scrf=(iefpcm,read) opt=gdiis			
ppn-oh ESR			

Symbolic Z-matrix:			
Charge = 0 Multiplicity = 2			
C	-0.87755 1.72044 -0.60551		
C	-0.66965 3.05078 -0.96605		
C	0.32364 3.80505 -0.33548		
C	1.11038 3.22447 0.65997		
C	0.90149 1.89274 1.02244		
C	-0.08925 1.13283 0.39295		
H	-1.63851 1.12472 -1.09678		
H	-1.2811 3.49977 -1.74422		
H	0.48191 4.84231 -0.61871		
H	1.88137 3.80676 1.15732		
H	1.51295 1.44153 1.80123		
C	-0.31443 -0.30591 0.80698		
H	0.24247 -0.50831 1.73342		
N	0.20141 -1.25924 -0.18231		
C	0.55863 -2.64108 0.22759		
H	0.79477 -2.5841 1.2968		
C	1.80099 -3.08754 -0.54718		
H	1.59842 -3.06056 -1.62135		
H	2.65213 -2.43002 -0.34108		
H	2.07455 -4.10966 -0.2649		
C	-0.63385 -3.58444 0.01741		
H	-0.37104 -4.60289 0.32477		
H	-1.49976 -3.2512 0.59584		
H	-0.90897 -3.59766 -1.04185		
O	-1.69661 -0.61091 0.99143		
H	-2.0989 0.14124 1.4557		
O	-0.05176 -1.05446 -1.42241		

APPENDIX C: Structural Details of DMPO/DMPO-OH

Cartesian coordinates of DMPO with DFT/B3LYP/6-31G*

Start DMPO			
echo			
charge 0			
geometry autosym units angstrom			
C	-0.194607	-0.0466734	0.383930
C	0.651491	0.915656	1.25798
H	0.129740	1.20520	2.19740
H	0.911435	1.85116	0.713995
C	1.93373	0.141003	1.58326
H	2.83807	0.691141	1.24537
H	2.00115	-0.0858319	2.66974
C	1.78314	-1.11898	0.814366
H	2.52889	-1.90669	0.778319
N	0.667426	-1.20301	0.191327
O	0.332124	-2.27361	-0.534168
C	-0.536567	0.586690	-0.974692
H	0.393125	0.845281	-1.52592
H	-1.12697	-0.118568	-1.59794
H	-1.13267	1.51248	-0.826888
C	-1.47916	-0.472301	1.11340
H	-2.05051	-1.20399	0.502762
H	-2.12596	0.411533	1.30274
H	-1.23109	-0.947403	2.08758
end library "6-31G*"			
ecce_print			
/home/jacob/nwchem_run/DMPO/ecce.out			
mult 1			
basis "ao basis" cartesian print			
H library "6-31G*"			
O library "6-31G*"			
C library "6-31G*"			

```
    default

   maxiter 50

end

task dft optimize
```

PCM structure for DMPO-OH at theDFT/B3LYP/6-31G*

```
#b3lyp/6-31G(d) scrf=(iefpcm,read) opt=gdiis
 --------------------------------------------
 1/14=-1,18=20,19=11,26=3,38=1,46=1/1,3;
 2/9=110,17=6,18=5,40=1/2;
 3/5=1,6=6,7=1,11=2,25=1,30=1/1,2,3;
 4//1;
 5/5=2,38=4,40=2200,42=-5,53=1,54=100/2;
 6/7=2,8=2,9=2,10=2,28=1/1;
 7/44=1/1,2,3,16;
 1/14=-1,18=20,19=11,46=1/3(1);
 99//99;
 2/9=110/2;
 3/5=1,6=6,7=1,11=2,25=1,30=1/1,2,3;
 4/5=5,16=2/1;
 5/5=2,38=4,40=2200,42=-5,53=1,54=100/2;
 7/44=1/1,2,3,16;
 1/14=-1,18=20,19=11,46=1/3(-5);
 2/9=110/2;
 6/7=2,8=2,9=2,10=2,19=2,28=1/1;
 99/9=1/99;
 -----------
 dmpo-oh PCM
 -----------
 Symbolic Z-matrix:
 Charge =  0 Multiplicity = 2
 C              0.1871   0.98357  -0.01029
 C              1.63592  0.51672   0.25629
 H              1.90805  0.73604   1.29582
 H              2.35492  1.03233  -0.38714
```

C	1.62652	-1.01007	0.01856
H	1.70014	-1.24701	-1.04768
H	2.4423	-1.52251	0.53539
C	0.24959	-1.46709	0.49788
H	0.25329	-1.77657	1.55626
N	-0.56743	-0.23393	0.39646
O	-1.83797	-0.33159	0.31055
C	-0.08383	1.26275	-1.49988
H	0.27145	0.44249	-2.13218
H	-1.15978	1.37533	-1.66307
H	0.41823	2.18513	-1.81239
C	-0.25649	2.168	0.85282
H	-1.32723	2.34985	0.71809
H	0.29004	3.07421	0.56945
H	-0.07294	1.96962	1.9142
O	-0.29497	-2.47578	-0.307
H	-1.2616	-2.3884	-0.19378

Isotropic Fermi Contact Couplings for DMPO-OH at DFT/B3LYP/6-31G*

Isotropic Fermi Contact Couplings

Atom	a.u.	MegaHertz	Gauss	10(-4) cm-1
1 C(13)	-0.00769	-8.64844	-3.08598	-2.88481
2 C(13)	-0.00067	-0.75554	-0.26959	-0.25202
3 H	-0.00004	-0.19060	-0.06801	-0.06358
4 H	-0.00023	-1.01497	-0.36217	-0.33856
5 C(13)	0.00195	2.19057	0.78165	0.73070
6 H	-0.00013	-0.58263	-0.20790	-0.19435
7 H	0.00029	1.29994	0.46385	0.43361
8 C(13)	-0.00782	-8.78791	-3.13575	-2.93133
9 H	0.01054	47.10771	16.80921	15.71344
10 N(14)	0.11779	38.05872	13.58030	12.69502
11 O(17)	0.07358	-44.60846	-15.91741	-14.87978
12 C(13)	0.01902	21.38302	7.63000	7.13261
13 H	-0.00045	-2.01586	-0.71931	-0.67242
14 H	-0.00061	-2.73754	-0.97682	-0.91315
15 H	0.00120	5.35870	1.91212	1.78747
16 C(13)	0.01284	14.43126	5.14944	4.81375
17 H	-0.00034	-1.50630	-0.53749	-0.50245
18 H	-0.00001	-0.04754	-0.01696	-0.01586
19 H	-0.00031	-1.37220	-0.48963	-0.45772
20 O(17)	0.00260	-1.57404	-0.56166	-0.52504
21 H	-0.00010	-0.46178	-0.16478	-0.15403

Cartesian coordinates of DMPO-OH with DFT/B3LYP/6-31G*

%chk=dmpo-oh.chk
%mem=250mb
%Nprocs=2
Will use up to   2 processors via shared memory.

#b3lyp/6-31G(d) scf=tight prop=epr

1/38=1/1;

2/17=6,18=5,40=1/2;

3/5=1,6=6,7=1,11=2,25=1,30=1/1,2,3;

4//1;

5/5=2,32=2,38=4,42=-5/2;

6/7=2,8=2,9=2,10=2,17=2,26=4,28=1/1,2;

99/5=1,9=1/99;

----

dmpo-oh EPR

Symbolic Z-matrix:

Charge = 0 Multiplicity = 2

C	0.1871	0.98357	-0.01029
C	1.63592	0.51672	0.25629
H	1.90805	0.73604	1.29582
H	2.35492	1.03233	-0.38714
C	1.62652	-1.01007	0.01856
H	1.70014	-1.24701	-1.04768
H	2.4423	-1.52251	0.53539
C	0.24959	-1.46709	0.49788
H	0.25329	-1.77657	1.55626
N	-0.56743	-0.23393	0.39646
O	-1.83797	-0.33159	0.31055
C	-0.08383	1.26275	-1.49988
H	0.27145	0.44249	-2.13218
H	-1.15978	1.37533	-1.66307
H	0.41823	2.18513	-1.81239
C	-0.25649	2.168	0.85282
H	-1.32723	2.34985	0.71809
H	0.29004	3.07421	0.56945
H	-0.07294	1.96962	1.9142
O	-0.29497	-2.47578	-0.307
H	-1.2616	-2.3884	-0.19378

```
#b3lyp/6-31G(d) scf=tight prop=epr

 ----------------------------------
 1/38=1/1;
 2/17=6,18=5,40=1/2;
 3/5=1,6=6,7=1,11=2,25=1,30=1/1,2,3;
 4//1;
 5/5=2,32=2,38=4,42=-5/2;
 6/7=2,8=2,9=2,10=2,17=2,26=4,28=1/1,2;
 99/5=1,9=1/99;
 -----------
 dmph-oh EPR
 -----------
 Symbolic Z-matrix:
 Charge =  0 Multiplicity = 2
 C              1.41075   1.02707   0.70396
 H              1.52644   0.99896   1.79364
 H              2.08373   1.78995   0.30575
 C              1.64316  -0.37153   0.09129
 H              2.48561  -0.89925   0.5477
 H              1.84302  -0.27429  -0.98155
 C             -0.04028   1.34249   0.35441
 H             -0.56679   1.94888   1.10326
 C              0.3098   -1.11232   0.29626
 H              0.29072  -1.59013   1.28829
 N             -0.66388   0.01041   0.32291
 O             -1.89874  -0.11196   0.01762
 C             -0.0547   -2.14567  -0.76274
 H              0.64385  -2.98834  -0.72227
 H             -1.06835  -2.51892  -0.59559
 H             -0.0129   -1.70376  -1.76408
 O             -0.11064   1.9507   -0.91951
 H             -1.04319   1.88457  -1.19156
 ----------------------------------------------------------------------
```

Cartesian coordinates of HMPO with DFT/B3LYP/6-31G*

Title "HMPO-1"			
Start HMPO-1			
echo			
charge 0			
geometry autosym units angstrom			
C	0.555701	-1.11842	-0.863836
H	1.60950	-1.61686	-0.963706
H	-0.0111940	-1.19702	-1.88430
C	0.723169	0.364196	-0.482509
H	1.33730	0.913560	-1.31314
C	-0.252644	-1.84151	0.229468
H	-0.379877	-2.96791	-0.0602403
H	0.314251	-1.76291	1.24994
C	-1.63969	-1.18544	0.360922
H	-2.40805	-1.59346	1.14326
N	-0.645862	1.01174	-0.352764
O	-0.756382	2.44275	0.00834573
C	1.46934	0.467652	0.860670
H	2.52313	-0.0307878	0.760800
H	1.59657	1.59405	1.15038
H	0.855207	-0.0817107	1.69130
end			
ecce_print			
/home/jacob/nwchem_run/Spin_trap/HMPO-			
1/ecce.out			
basis "ao basis" cartesian print			
H library "6-31G*"			
O library "6-31G*"			
C library "6-31G*"			
N library "6-31G*"			
END			

```
dft
  mult 1
  XC b3lyp
  mulliken
end

driver
  default
  maxiter 30
end
task dft optimize
```

Isotropic Fermi Contact Couplings for HMPO-OH at DFT/B3LYP/6-31G*

Isotropic Fermi Contact Couplings

Atom	a.u.	MegaHertz	Gauss	10(-4) cm-1
1 C(13)	-0.00056	-0.62991	-0.22477	-0.21012
2 H	0.00045	2.00386	0.71503	0.66841
3 H	0.00009	0.42002	0.14987	0.14010
4 C(13)	0.00280	3.14605	1.12259	1.04941
5 H	0.00028	1.26206	0.45034	0.42098
6 H	-0.00026	-1.17572	-0.41953	-0.39218
7 C(13)	-0.00343	-3.85921	-1.37706	-1.28729
8 H	0.00417	18.64097	6.65156	6.21796
9 C(13)	-0.01244	-13.98752	-4.99110	-4.66573
10 H	0.01324	59.19310	21.12158	19.74469
11 N(14)	0.10063	32.51481	11.60210	10.84577
12 O(17)	0.07608	-46.12064	-16.45699	-15.38419
13 C(13)	0.01071	12.03976	4.29609	4.01603
14 H	-0.00026	-1.16705	-0.41643	-0.38928
15 H	-0.00033	-1.45342	-0.51862	-0.48481
16 H	-0.00006	-0.27343	-0.09757	-0.09121
17 O(17)	0.01293	-7.84126	-2.79796	-2.61556
18 H	-0.00046	-2.06752	-0.73774	-0.68965

PCM structure for HMPO-OH at theDFT/B3LYP/6-31G*

```
#b3lyp/6-31G(d) scrf=(iefpcm,read) opt=gdiis
 --------------------------------------------
 1/14=-1,18=20,19=11,26=3,38=1,46=1/1,3;
 2/9=110,17=6,18=5,40=1/2;
 3/5=1,6=6,7=1,11=2,25=1,30=1/1,2,3;
 4//1;
 5/5=2,38=4,40=2200,42=-5,53=1,54=100/2;
 6/7=2,8=2,9=2,10=2,28=1/1;
 7/44=1/1,2,3,16;
 1/14=-1,18=20,19=11,46=1/3(1);
 99//99;
 2/9=110/2;
 3/5=1,6=6,7=1,11=2,25=1,30=1/1,2,3;
 4/5=5,16=2/1;
 5/5=2,38=4,40=2200,42=-5,53=1,54=100/2;
 7/44=1/1,2,3,16;
 1/14=-1,18=20,19=11,46=1/3(-5);
 2/9=110/2;
 6/7=2,8=2,9=2,10=2,19=2,28=1/1;
 99/9=1/99;
 -----------
 dmph-oh PCM
 -----------
 Symbolic Z-matrix:
 Charge =  0 Multiplicity = 2
 C             1.10971   1.31147  -0.45242
 H             1.16197   1.55456  -1.5189
 H             1.89425   1.86845   0.06492
 C            -0.30525   1.59407   0.09773
 H            -0.72917   2.52428  -0.2884
 H            -0.27831   1.66108   1.19124
 C             1.29218  -0.19417  -0.27127
 H             1.88165  -0.67902  -1.05758
 C            -1.1291    0.36699  -0.32277
 H            -1.50642   0.49834  -1.34804
```

N	-0.09107	-0.69249	-0.36938
O	-0.3551	-1.93791	-0.48567
C	-2.28743	-0.01666	0.59123
H	-3.06711	0.75056	0.5486
H	-2.72139	-0.96956	0.27605
H	-1.94957	-0.11262	1.62893
O	1.8481	-0.461	1.00348
H	1.92696	-1.42756	1.0913

VITA

JACOB FOSSO TANDE

Personal Data: Date of Birth: January 26, 1976

Place of Birth: Bamougoum, Republic of Cameroon

Marital Status: Single

Education: Public and private schools, Bafoussam, Republic of Cameroon

Douala University, Republic of Cameroon

     Diploma in Physics, 1999

University of Buea, Republic of Cameroon

     Chemistry, Bsc. 2002

East Tennessee State University, Tennessee

     Chemistry, M.S., 2007

Professional

Experience: Library Assistant, University of Buea, Republic of Cameroon

     Buea, Republic of Cameroon 1999 - 2002

Mathematics, Physics and Chemistry Instructor M.L.K.B

     Bafoussam, Republic of Cameroon 2002 – 2005

Graduate Assistant, East Tennessee State University (ETSU),

     Department of Chemistry, 2005 – 2007

Physics Instructor, Upward bound program, ETSU

     Johnson City, Tennessee, Summer 2007